

# CUAHSI's Hydroinformatics Innovation Fellowship

## Multi-Source and Multi-Temporal Google Earth Engine App for Emergency Flood Mapping

Principal Investigator: Ebrahim Hamidi, Ph.D. Candidate at The University of Alabama

Co-PI: Brad G. Peter, Assistant Professor, Department of Geosciences, University of Arkansas

Final Report – January 2024



**CUAHSI**  
allied for water science  
[www.cuahsi.org](http://www.cuahsi.org)

## Table of contents

Narrative of highlights .....	2
Abstract:.....	3
1- Introduction: .....	3
2- Fellowship Objectives: .....	5
3- Research Product:.....	5
4- The App Flood Monitoring Capabilities Testing .....	7
Addressing First Objective: .....	7
Addressing Second Objective:.....	12
Addressing Third Objective: .....	16
5- Additional Features For Expert Users .....	18
6- Research Challenges and Limitations.....	22
7- Links Ror the App's Code and Dissemination Documents.....	23
8- Acknowledgement: .....	23
9- Test Case Examples: .....	24
10- References: .....	34
Appendix I: More Detail on Flood Extraction From SAR Index Images .....	35
Appendix II: Poster Presentation at The AGU 2023 Fall Meeting .....	37

## Narrative of highlights

Floods, common natural disasters worldwide, resulted in approximately \$40 billion in losses between 2011 and 2015, as reported by the Financial Management of Flood Risk [1].

Science and technology advancements provide alternatives for managing natural disasters such as floods. Satellite-based flood inundation mapping is crucial for emergency responders, aiding crisis managers in monitoring and managing floods. It enhances situational awareness, identifying areas requiring immediate action across large geographical areas, expediting relief response activities.

Remote sensing is widely employed not only for flood inundation mapping but also for assessing flood impact, offering a comprehensive review to address diverse stakeholder needs [2]. These stakeholders have specific requirements aligned with particular objectives, serving various purposes.

- Flood monitoring
- Strategies for preventing and mitigating flood risks
- Emergency response planning
- Prioritizing preventive actions through classifying flooded areas
- Estimating the population at risk
- Land-use planning and management
- Public awareness campaigns
- Providing information for the insurance sector

Due to the unpredictable nature of flooding and the slow retrieval rate of satellite images, local implementation faces limitations. Relying solely on remotely sensed images poses challenges in fully capturing the scope of flood monitoring. This has prompted research into integrating multiple sources for improved flood mapping [2], [3].

This research study introduces an App that uses multi-source and multi-temporal remote sensing data for fast flood monitoring. This App provides tools to facilitate flood monitoring tasks by defining a flood period and drawing a boundary to observe the flood extent conditions in their area of interest. Through this App, our aim is to empower decision-makers, first responders, scientists, and other stakeholders with clear, useful information, enabling them to better understand, prepare for, and respond to treacherous flooding hazards. This information is crucial, considering the populations, infrastructure facilities, urban area, and cropland at risk.

**Abstract:**

Recent studies suggest that global warming will lead to a greater chance of extreme flooding in the coming decades, doubling every five years in the near future. Coastal regions, being densely populated areas, are highly vulnerable to flooding due to various drivers such as extreme rainfall and tropical cyclones. Therefore, identifying efficient and accurate models for mapping floods is key in flood risk assessment. While remotely sensed observations have provided researchers with decades of continuous and reliable data for extracting flood information, it is important to note that relying solely on single-source remote sensing data may not provide a comprehensive solution for urgent flood monitoring. Satellite revisit cycles, spatial resolution, weather conditions, and solar reflectance dependency, as well as sensor defects, are a number of remote sensing limitations that can hinder flood mapping progress.

Multi-source methods can address part of the limitations inherent in single-source methods. These methods can cope with the drawbacks of satellite data while leveraging their advantages. For example, using multi-source optical/SAR imagery can provide abundant spectral information and highly accurate water extraction from the optical imagery, thereby benefiting the SAR images all-weather and day-night operation capabilities for flood mapping. In this study, we build on our previous research and introduce an App that leverages state-of-the-art remote sensing resources and the capability of the Google Earth Engine (GEE) platform to produce a rapid estimation of floods using an advanced multi-source remote sensing approach that is geographically generalizable. Then, this GEE App extracts multidisciplinary information from the final flood map for responsible responders to adopt flexible measures based on the types of land-use and land-cover affected.

This tool will be among the first user-friendly GEE Apps that produce flood extent maps at a scale that will help emergency responders as well as the scientific community with rapid and reliable flood inundation information and improves the current methods of flood mapping.

**1- Introduction:**

Recent studies suggest that sea level rise will lead to a greater chance of extreme flooding in the coming decades, doubling every five years in the near future [4]. A large population of the world's citizens resides in coastal regions [5], [6]. These densely populated areas are highly vulnerable to flooding due to drivers such as extreme rainfall, tropical cyclone, and tsunamis [7].

The United States of America's long coastline exemplifies significant exposure to coastal flooding. Low-gradient coastal regions, such as the Atlantic and Gulf coasts of the U.S. are susceptible to damaging and catastrophic flooding from both large overland precipitation events and storm surges from tropical storms. Floodwater extent prediction and monitoring are critical to enabling responsible authorities to evaluate the hazard risk and respond efficiently and immediately to the potential threat of flooding [8]. Therefore, identifying efficient and accurate models for mapping floods is key in flood risk assessment [9].



Fig. 1: Flood hazard is the consequence of meteorological drivers.

In recent decades, researchers have been studying flood hazard mitigation using remote sensing data. Satellites provide decades of continuous and reliable data that researchers can translate into meaningful and applicable flood information for responsible authorities [8]. Optical satellites have been collecting image data since the 1970s and producing multi-spectral images that are very useful for flood mapping. However, these image data are highly affected by meteorological and diurnal cycles. Synthetic-Aperture Radar (SAR) satellites can be another alternative for flood monitoring since the radar satellites produce high-resolution data, regardless of weather conditions and time of day [10]. Nevertheless, flood detection and monitoring with SAR data face some challenges [11]; for instance, radar shadow due to buildings could incorrectly classify dry areas as flooded ones [12], and imagery roughness produced by wind and heavy rainfall can hinder flood delineation [13].

It is clear that single-source remote sensing data do not offer a complete solution for urgent flood monitoring. Satellite revisit cycles, spatial resolution, weather conditions, and solar reflectance dependency, as well as sensor defects, are a number of remote sensing limitations that can hinder flood mapping progress. Furthermore, time is critical for urgent disaster management and decision-makers cannot wait for perfect high-quality images. Multi-source methods can address part of the limitation inherent in single-source methods [14], [15]. These methods can cover the drawbacks of each remote sensing data and leverage their advantage. For example, using multi-source optical/SAR imagery leverages the abundant spectral information and enables highly accurate water extraction from the optical imagery and takes the benefits of SAR images all-weather and day-night operation capabilities for flood mapping [14]. Combining multi-temporal and multi-source remote data for flood inundation analysis is a new method [3], [12]; however, this advanced approach needs further exploration on providing automatic, large-scale, and high-precision floodwater extraction [14].

Advanced remotely sensed methods have the capability of equipping responsible authorities with valuable information to adopt preventive measures and reduce the consequences of floods (e.g., flood forecasting and evacuation plans, warning systems, and reduction of exposed population and property) [16]. Further research in this context is critical to producing reliable information for emergency responders for analyzing, evaluating, and designing flood-risk-management practices.

This research develops a user-friendly GEE App to provide decision-makers and responsible authorities with accurate and rapid flood monitoring tools. This App uses multi-temporal and multi-source satellite images for flood mapping. The approach will address some of the shortcomings of current methods for flood mapping including, 1) mapping the extent of floods regardless of the weather condition and daytime (SAR data), 2) detecting floods where/when SAR fails (optical images), 3) defining optimum thresholds for extraction of flooded pixels (from SAR indices images) and 4) extracting multi-disciplinary information from the final flood maps to categorize the affected areas and provide strategic information for flood emergency response planning.

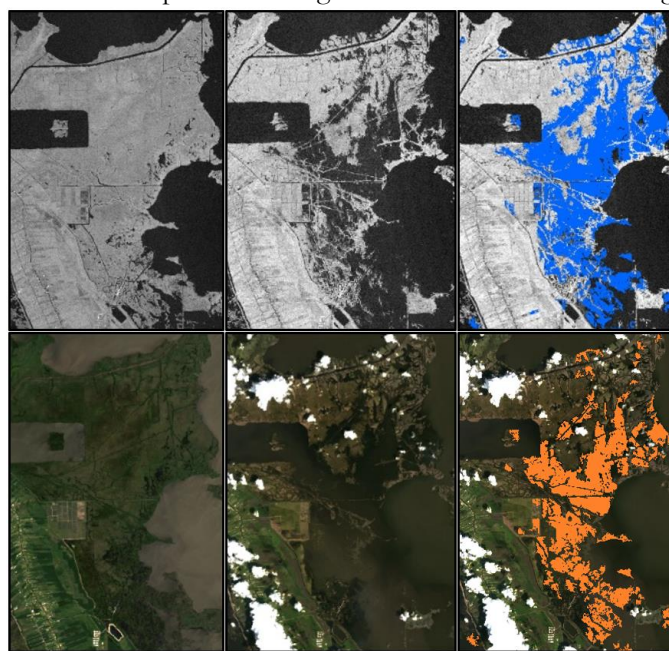


Fig. 2: Flood extraction from SAR and optical satellite datasets.

## 2- Fellowship Objectives:

The main research objectives of this study, as outlined in the research proposal, are as follows:

**First Objective: Provide a programmatic SAR Change Detection flood monitoring tool that is independent of meteorological and diurnal cycles.**

This study uses SAR data that can capture the flood independent of the solar reflection. A multi-temporal change detection and thresholding approach is applied using SAR indices such as the Normalized Difference Flood Index, Difference Image Index, and Raito Index. In this stage, the App provides a quick estimation of flood by constant pre-defined thresholding values using the combination of different SAR indices and produces a rapid estimation of flood extent during and after floods. This GEE App outweighs the traditional methods of flood mapping using remote sensing data by expediting the flood extraction procedure without the need to download data or use local computation resources. It is worth mentioning that monitoring various study areas is as simple as drawing a new polygon in this GEE App.

**Second Objective: Combine optical and SAR flood mapping approaches to increase the reliability and geographic generalizability of the final flood extent maps.**

SAR drawbacks include radar shadows being incorrectly classified as water and imagery ‘roughness’ from wind and heavy rainfall leading to underestimation of flooded areas. These shortcomings can be addressed in part by integrating both SAR and optical datasets. Although optical images can be affected significantly by atmospheric and daytime conditions, these images provide valuable multi-spectral data for flood mapping. Moreover, the selection of appropriate threshold values to extract flooded pixels from SAR indices images is not a straightforward task. This App proposes a multi-source and multi-temporal remote sensing approach that helps improve the accuracy of the final flood map by providing optimum threshold values for extracting flooded pixels compared with the methods that used constant threshold values. This approach integrates SAR and optical images and provides an automated coded framework that is not computationally demanding and expedites the procedure for emergency flood mapping.

**Third Objective: Provide multidisciplinary flood hazard information for geographically strategic emergency response plans in near real-time.**

This project leverages the significant capabilities of GEE to extract multidisciplinary information from flood maps (e.g., Basic Demographic Characteristics (GPWv411) and USGS National Land Cover Database, 2019) to assess further critical supplementary information. The output of this integrated framework expands the agenda on flood-risk management to include essential flood consequences on economic, sociological, and geopolitical elements. This tool casts light on the specific land-use/land-cover types affected by flood events to better evaluate and respond to areas in a more targeted manner, i.e., urban inundation and exposed population, at-risk humans and vital infrastructures, affected industries, damaged agricultural products, and negative impacts on wildlife and the environment. With the availability of a wide variety of near real-time remote sensing data collections and demographic datasets, as well as high-performance cloud computing, GEE is an excellent medium for elucidating the intersection of floods and affected populations.

This study aims to monitor global-scale flood extents by addressing the stated research objective through the development of a user-friendly Google Earth Engine (GEE) App. The resulting product will offer rapid and reliable flood inundation information, benefiting both emergency responders and the scientific community, thereby enhancing current flood mapping methods. Throughout this report, the methodology behind the GEE Fast Flood Monitoring Tool is outlined, demonstrating how users can effectively employ the App for rapid flood mapping. Specific details on the App's design are provided, emphasizing its user-friendly features for non-expert users. Additionally, the App is structured to accommodate more experienced users, enabling detailed flood extent analyses. The report includes a simple example illustrating effective App utilization and presents several real-world examples to show the tool's practical applications.

## 3- Research Product:

This product of this study is a user-friendly Google Earth Engine App (GEE App) to monitor global scale flood extents. This Fast Flood Monitoring Tool (FFMT) product will help emergency responders as well as the scientific community with rapid and reliable flood inundation information and improves the current methods of flood mapping. Figure 3 summarizes the methodology embedded in this App through a graphical flowchart.

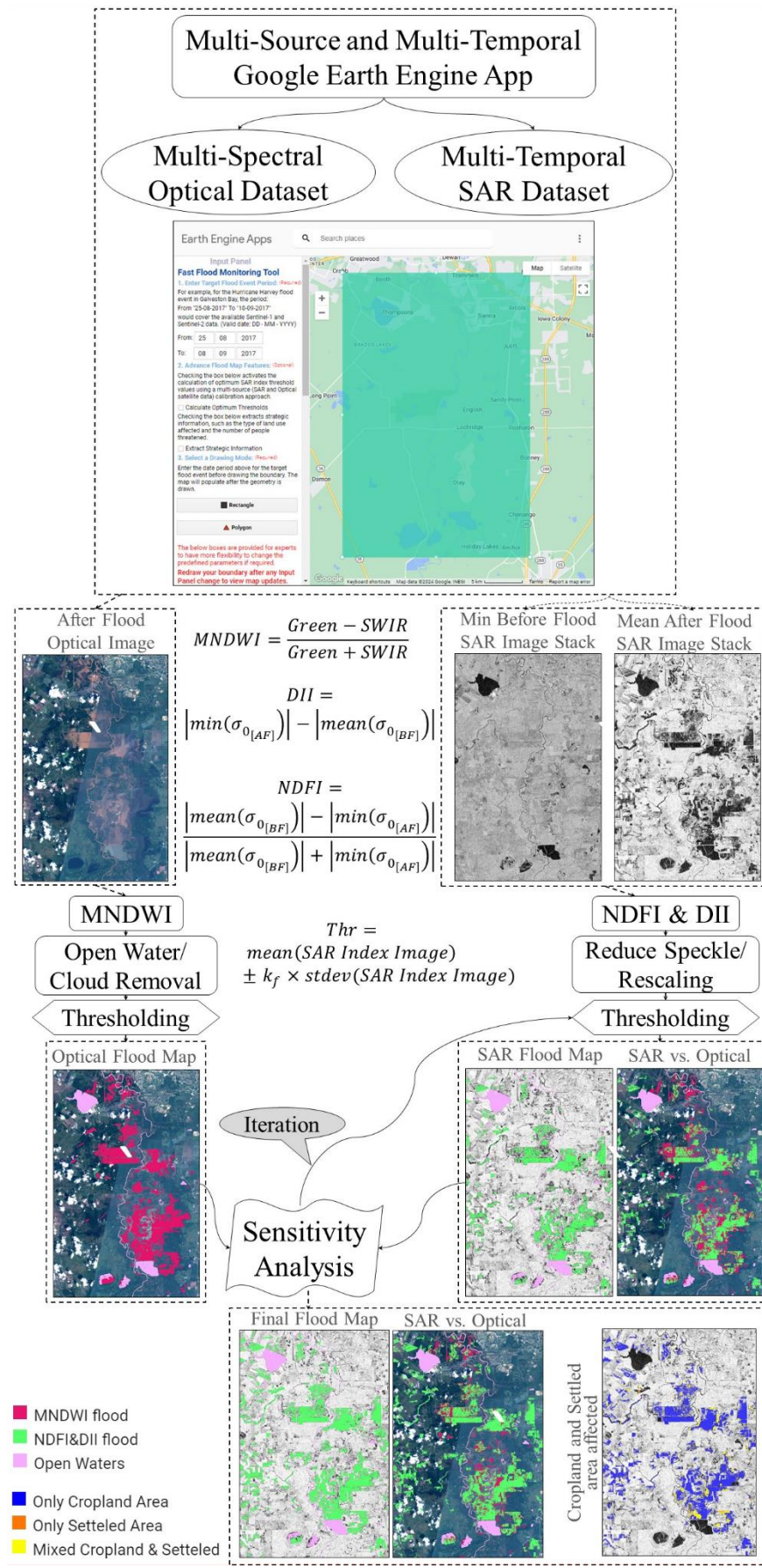


Figure 3: GEE App methodology flowchart

This App integrates multi-source and multi-temporal remote sensing datasets to achieve highly precise and efficient floodwater extraction. Initially, multi-temporal SAR images are utilized to employ a change detection technique, generating SAR index images that highlight inundated areas post-flood, including the normalized difference flood index (NDFI) and the difference image index (DII). This inundation map can be considered as the primary estimation of flood extent estimation. Subsequently, for enhancing the generated flood map, the App leverages available Sentinel-2 optical images (if any) to conduct an automated sensitivity analysis and identify the optimal SAR index threshold values for flood extraction. Finally, employing the calculated optimal thresholds, the ultimate flood maps are extracted from SAR index images. Using the flood map extracted from previous steps, the App provides crucial data, presenting insights into the number of individuals facing potential threats and quantifying the impact on both urban areas and cropland.

#### 4- The App Flood Monitoring Capabilities Testing

**Addressing First Objective:** *Provide a programmatic SAR Change Detection flood monitoring tool that is independent of meteorological and diurnal cycles.”*

In this study, we leveraged near real-time Sentinel-1 Level-1 Ground Range Detected (GRD) imagery, which is accessible through the GEE dataset "COPERNICUS/S1\_GRD" with 10-meter spatial resolution and a temporal resolution of 12 days (6 days when coupling both Sentinel-1 satellites in the constellation). This radar dataset is very useful for flood detection as it provides beneath-cloud imagery regardless of weather conditions and time of day [10], [17], [18].

The App uses a multi-temporal flood detection method that considers both pre-flood as a baseline and post-flood SAR data to provide more reliable flood maps [19], [20], [21], [22], [23], [24]. We utilize Vertical-Horizontal (VH) polarization, ascending pass direction, and SAR imagery in interferometric wide (IW) mode. Furthermore, we employ the U.S. Geological Survey 3D Elevation Program (3DEP) 10-meter spatial resolution Digital Elevation Model ("USGS/3DEP/10m") to filter out steep areas with slopes exceeding 5° [25]. This step masks the steeper slopes and therefore removes any pixels in the SAR image that may show a change in brightness due to the angle of signal return from hills and slopes [26]. The removal of these bright pixels is important for the calculation of the local statistics during thresholding; however, this step may be unnecessary for regions with relatively flat topography. Moreover, to eliminate permanent water features and isolate flooded regions, we rely on the JRC Global Surface Water Mapping Layers, version 1.1 ("JRC/GSW1\_0/GlobalSurfaceWater").

Figure 4 displays the initial screen of the Fast Flood Monitoring Tool (FFMT) App. On the left side of the App, an input panel outlines two necessary steps for users to initiate the engine behind the GEE App, which is further detailed in Figure 5. The first step is to specify the period of the target flood event ([1. Enter Target Flood Event Period](#)) and the second one is to draw a boundary around the area under study ([3. Select a Drawing Mode](#)) to extract flooded pixels from available Sentinel-1 and Sentinel-2 satellite data. The “[2. Advance Flood Map Features:](#)” section of the **Input Panel** is optional and will be explained later in this report. This hyperlink facilitates access to the App (<https://turnkey-aleph-386916.projects.earthengine.app/view/geefastfloodmonitoring>).

##### [1. Enter Target Flood Event Period](#) (Required)

Users are required to specify the **start date** and **end date** of the target flood event in the boxes located in front of the “**From:**” and “**To:**” using the “DD - MM - YYYY” format (Figure 5). For example, for the Hurricane Harvey flood event in Galveston Bay, the period:

**From:** “25-08-2017”

**To:** “08-09-2017”

would cover the available Sentinel-1 and Sentinel-2 data for this flood event.

##### [2. Advance Flood Map Features:](#) (Optional)

This step is optional and will be explained later in this report.

##### [3. Select a Drawing Mode](#) (Required)

The App offers two options for users to define the study area boundary: “**Rectangle**” for a rectangular shape and “**Polygon**” for custom shapes drawn by interacting with the map interface (see Figure 5). After defining the period for the target flood event, the user needs to draw a boundary around the area of interest. The map will populate once the geometry is drawn.

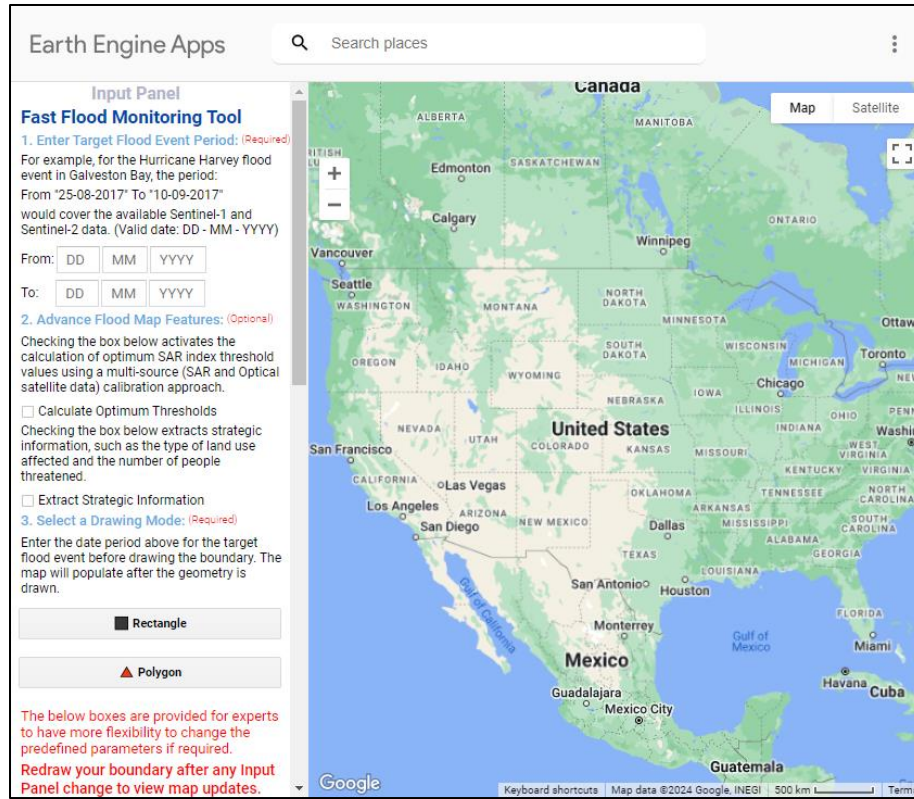


Figure 4: GEE App welcome panel which is available here: [GEE FFM \(earthengine.app\)](https://earthengine.app)

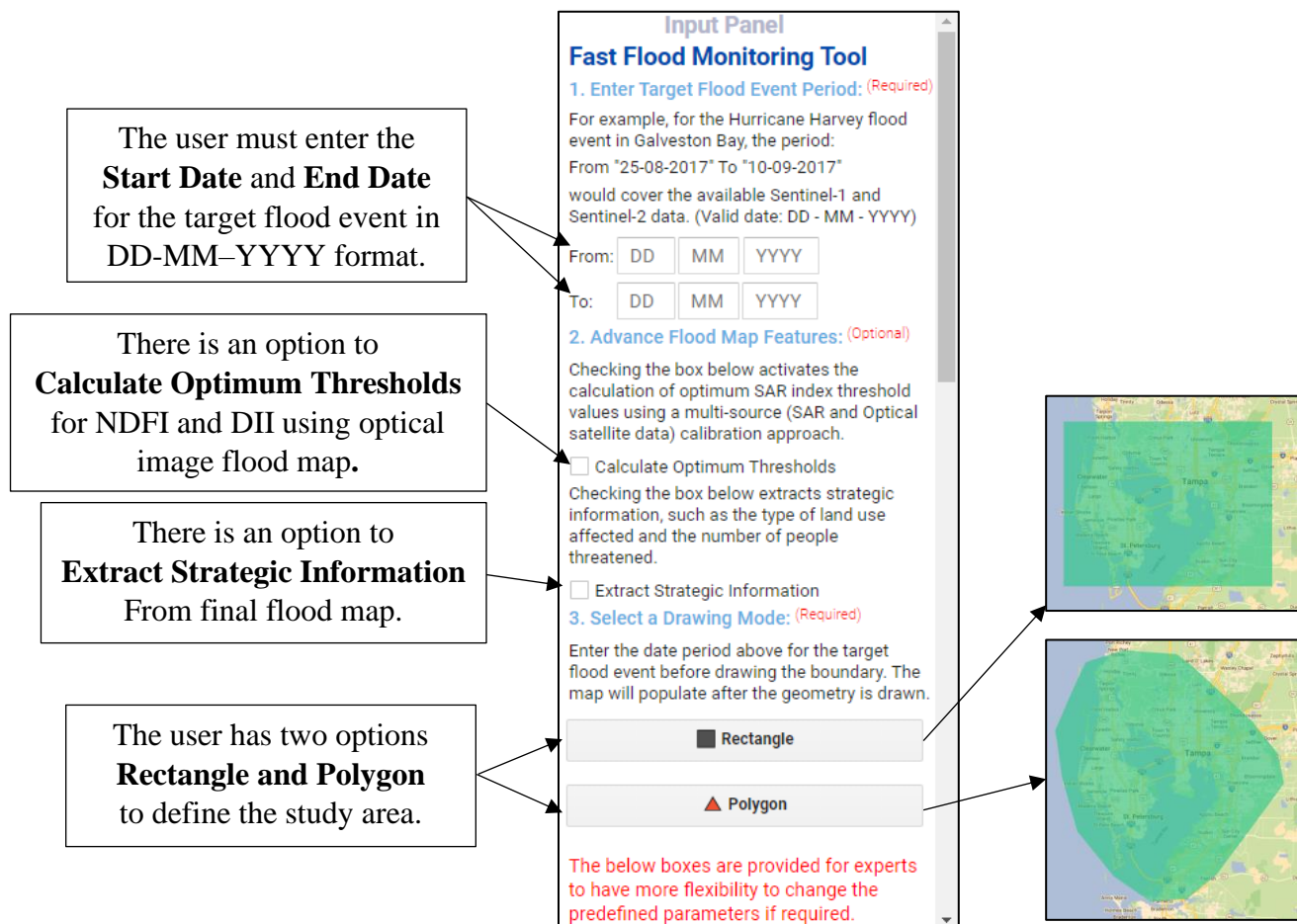


Figure 5: The Input Panel interface of the GEE App, displaying the necessary parameters to initiate the App engine.

We test the App's flood monitoring capabilities by demonstrating its advantage in mapping the flood that occurred after Hurricane Harvey in the south of the city of Houston. To extract post-hurricane flooded areas, we input August 25, 2017, as the **Flood Event Start Date** and September 08, 2017, as the **Flood Event End Date** (see Figure 6). In this test case, we leave the two boxes in the “**2. Advance Flood Map Features:**” unchecked and will provide an explanation of these boxes in the subsequent sections. Additionally, we zoomed in on the southern area of Houston and used the Rectangular button to draw a rectangle around the Brazos River, which continues to flow toward the Gulf of Mexico. We will illustrate how these inputs contribute to flood mapping. Figure 6 provides a visual representation of these steps.

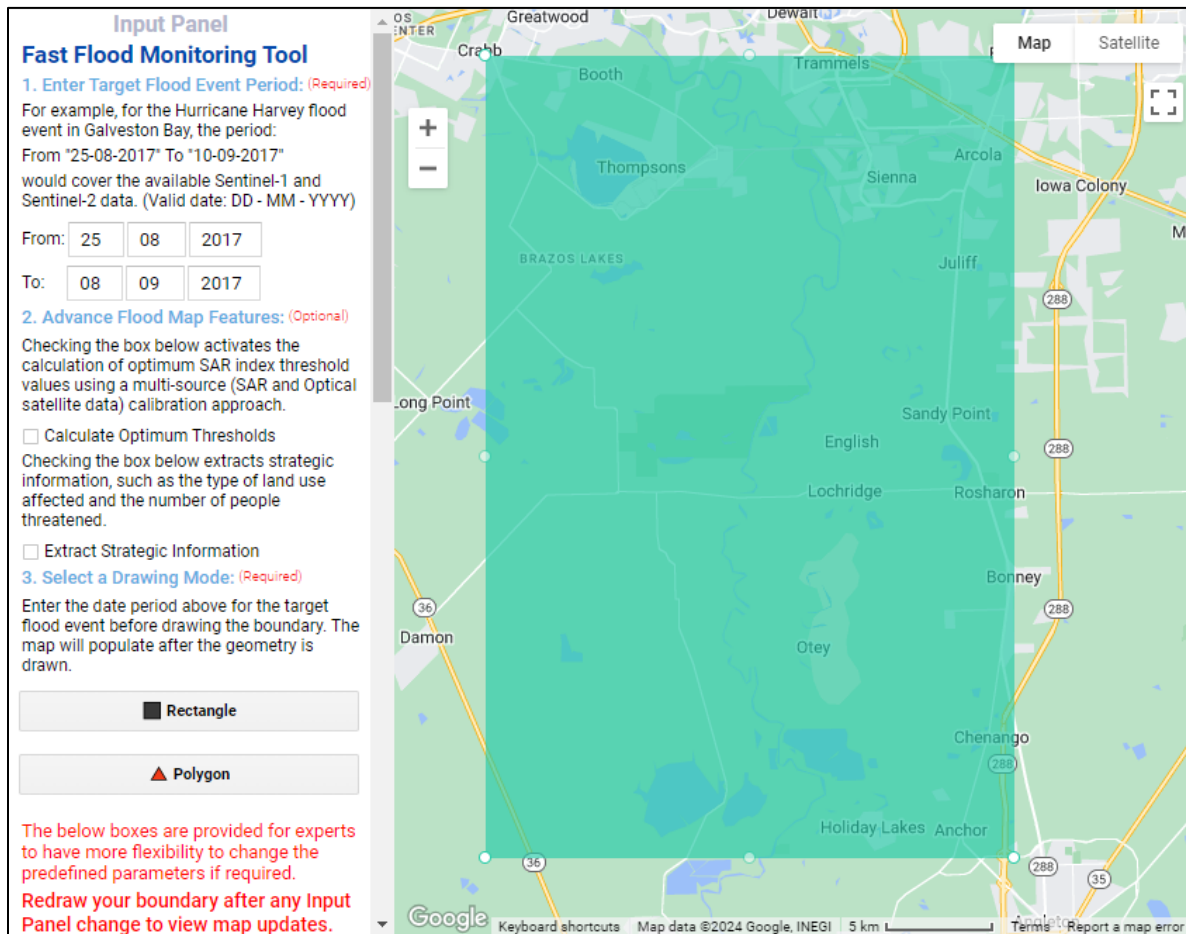


Figure 6: Assessing a flood monitoring App for the flood that occurred after Hurricane Harvey in the south of Houston.

Once the study area is selected, the App initiates dataset preparation. It utilizes the Sentinel-1 data source for both pre-flood and post-flood conditions, collecting reference and flood images, respectively. To gather the flood images, the App uses the period defined by the user in the App’s **Input Panel** (e.g., images between "25-08-2017" and "08-09-2017" for the flood after Hurricane Harvey in the southern part of the city of Houston).

However, the App automatically utilizes a predefined reference period, set between "01-06-2017" and "15-06-2017," to collect reference images. This period was defined to enhance the App’s usability for non-expert users. While this predefined period simplifies the process, expert users have the option to modify the reference period within the **Input Panel** (see “Additional features for expert users” section of this report). This flexibility allows them to refine the assessment for flood extent with more detailed information.

After collecting flood and reference image collections, the App creates a reference flood image stack by calculating the mean backscattering pixel values from the images collected as reference images, which are used to identify pre-flood conditions. Subsequently, the App generates a post-flood image stack by computing the minimum backscattering pixel values from the flood image collection. This method effectively captures the maximum flood extent using available post-flood images. Users can access these datasets through the “**Layers**” toolbar located at the top-right corner of the screen.

Figure 7 depicts the “Layers” toolbar and the generated maps. Also, users can view the pre-flood and post-flood image stacks by checking the box next to each map. For example, in the test case of Hurricane Harvey’s flood in the south of the city of Houston, Figures 8a and 8b show the reference image stack (mean SAR image before the flood) and the flood image stack (minimum SAR image after the flood), respectively. The App utilizes these image stacks to calculate SAR-derived indices.



Fig. 7: The “Layers” toolbar, on the top-right corner of the screen for viewing the maps.

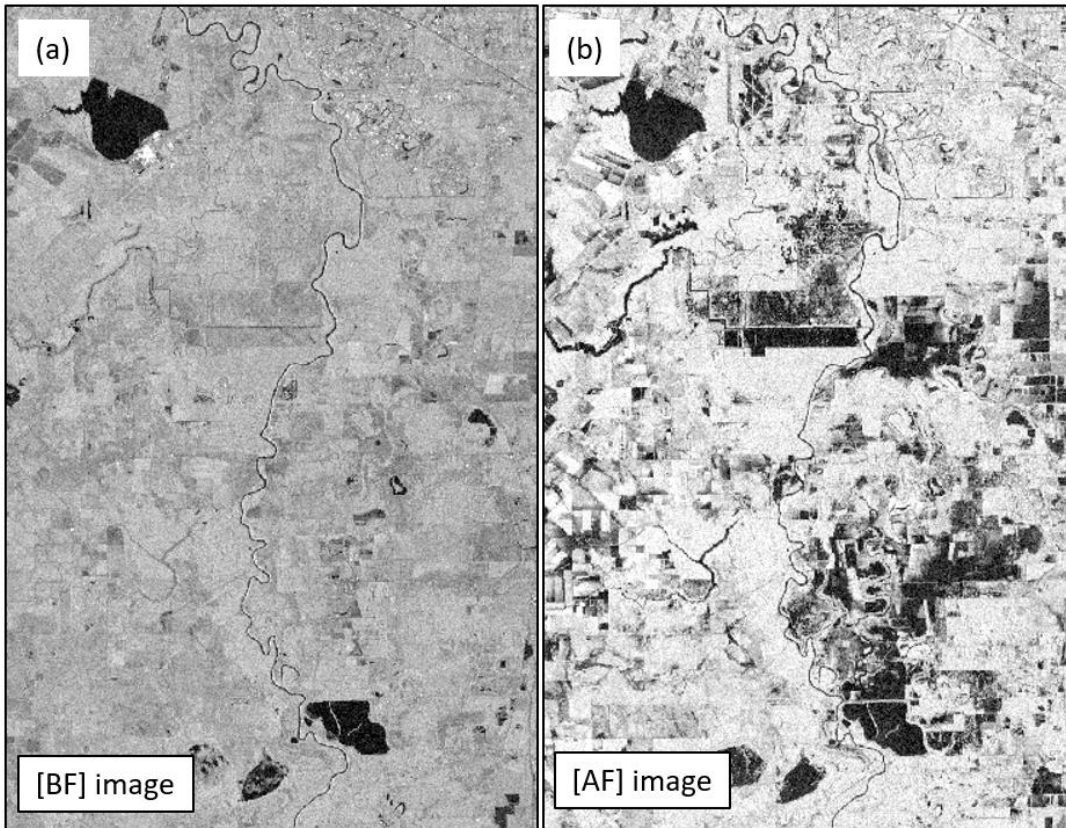


Figure 8: SAR data (a) mean pixel values from pre-flood SAR Images, and (b) minimum pixel values from post-flood SAR Images.

The Normalized Difference Flood Index (NDFI) and Difference Image Index (DII) are the indices that are used in this App to delineate the flooded pixels from multi-temporal image stacks. The NDFI and DII images are generated using equations (1) and (2), respectively.

$$NDFI = \frac{|mean(\sigma_0_{[BF]})| - |min(\sigma_0_{[AF]})|}{|mean(\sigma_0_{[BF]})| + |min(\sigma_0_{[AF]})|} \quad (1)$$

$$DII = |min(\sigma_0_{[AF]})| - |mean(\sigma_0_{[BF]})| \quad (2)$$

In these equations,  $\sigma_0_{[BF]}$  and  $\sigma_0_{[AF]}$  are the backscatter coefficient of SAR imagery before flood [BF] and after flood [AF], respectively [3], [21], [27]. Then the calculated NDFI and DII images are normalized to a 0-1 scale. In this App, the threshold values ( $Thr$ ) for extracting flooded pixels from NDFI and DII images are determined using ( $k_f$ ) standard deviations from the mean of the SAR index image pixel values as described in equation (3) [3], [20], [21].

$$Thr = mean(SAR\ Index\ Image) \pm k_f \times stdev(SAR\ Index\ Image) \quad (3)$$

In this formula, a negative sign is applied for NDFI, classifying pixel values below the threshold as representing flooded areas. Conversely, for DII in equation (3), a positive sign is used, categorizing pixel values exceeding the threshold as depicting flooded regions.

Now, we demonstrate how this methodology is applied in the App. With pre-flood and post-flood image stacks ready, the App employs equations (1) and (2) to generate NDFI and DII images, respectively. After generating NDFI and DII images, calculating the mean and standard deviation of pixel values for these SAR index images (NDFI and DII) becomes straightforward. Only the  $k_f$  value remains unknown in equation (3). In existing literature, several studies have proposed using a threshold of 1.5 as a reliable value for identifying flooded pixels in SAR index images [20], [21], [27], [28], [29]. Therefore, the App adopts the default value of 1.5 for the  $k_f$  coefficient in equation (3) to calculate threshold values and extract flooded pixels from SAR index images. However, this value can be modified in the **Input Panel** by expert users seeking more advanced flood mapping options (see “Additional features for expert users” section of this report).

After calculating the threshold values using equation (3), the App extracts flooded pixels from NDFI and DII images. Flood extent maps generated through the previous steps necessitate certain postprocessing adjustments. Initially, the JRC Global Surface Water Mapping Layers are utilized to mask out permanent water land cover. Following this, the USGS 3DEP DEM is employed to eliminate regions with slopes exceeding 5°, where the occurrence of floods would be improbable [25]. Ultimately, noise in the resulting imagery is minimized by the application of a smoothing filter, aimed at reducing the speckle effect associated with radar imagery. Subsequently, the App merges the flood maps extracted from NDFI and DII to decrease the chance of missing flooded pixels (reducing errors of omission) and provides the final flood map for the user. Users can view the final flood map by checking the box next to “**Combined NDFI&DII Flood**” in the “**Layers**” toolbar. Figure 9 illustrates the result of merged layers. For expert users who wish to view floods extracted by NDFI and DII separately, there is an option in to “**Display NDFI and DII Flood Map Results**” in “**I. Display Additional Map and Graphics**” section of the **Input Panel**. A more detailed explanation is provided in “**Appendix I: More detail on flood extraction from SAR index Images**”.

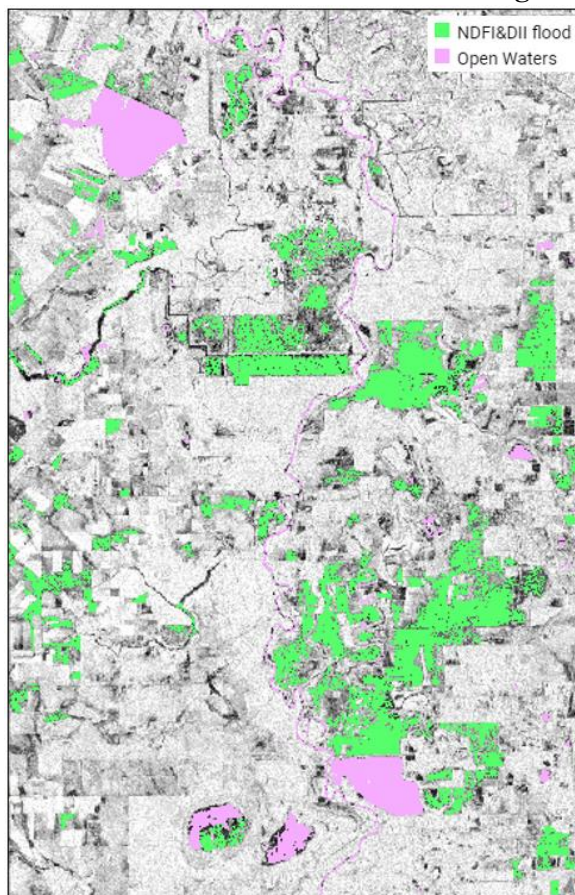


Figure 9: Result of merging two flooded areas extracted from NDFI and DII.

Utilizing the final flood extent map, the App provides information about the flood in the **Results Panel**. Additionally, this panel summarizes some of the input data defined by the user and provides details regarding the

earliest and latest available Sentinel-1 and Sentinel-2 data for the specified flood event period. For instance, as illustrated in Figure 10, the reported flooded extent map for the selected area after Hurricane Harvey is 99.45 square kilometers.

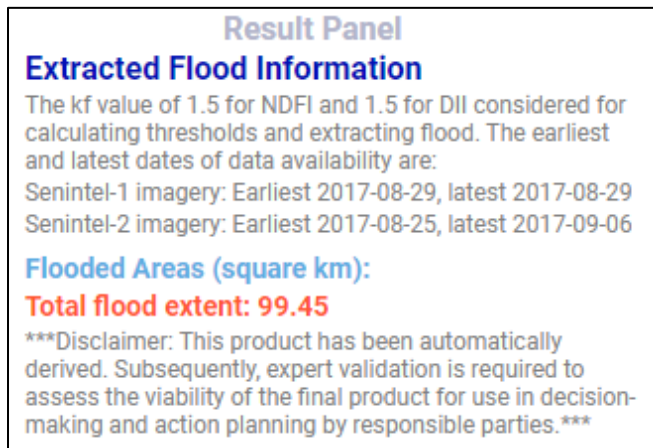


Figure 10: The output panel interface of the App.

Users may choose to discontinue using the App and utilize the extracted flood map for adapting flood mitigation measures or for more scientific analyses. Additionally, they can explore additional features of the map, as outlined below.

**Addressing Second Objective:** “*Combine optical and SAR flood mapping approaches to increase the reliability and geographic generalizability of the final flood extent maps.*”

As mentioned earlier, in equation (3), the default value for the  $k_f$  coefficient is typically set to 1.5, as demonstrated in numerous studies [20], [21], [27], [28], [29]. However, this constant threshold value may not always be suitable, leading to the failure of extracting flooded pixels across various indices and geographical locations [3]. Therefore, this application performs a sensitivity analysis on the  $k_f$  coefficient using available optical images to determine the threshold value that yields the highest agreement in extracting flooded pixels from SAR index images.

For conducting a sensitivity analysis, the App utilizes post-flood optical imagery (Sentinel-2 data) for the identification of inundated regions, employing the Modified Normalized Difference Water Index (MNDWI) [27], [28] as outlined in equation (4).

$$MNDWI = \frac{\text{Green Band} - \text{SWIR Band}}{\text{Green Band} + \text{SWIR Band}} \quad (4)$$

In this equation, Band 3 represents the Green Band, and Band 11 corresponds to the Short-Wave Infrared (SWIR) Band in the Sentinel-2 dataset. The MNDWI stands as a state-of-the-art optical index for discerning bodies of water in optical satellite image analysis, mainly due to their distinct absorption of Short-Wave Infrared (SWIR) radiation.

One of the strengths of this App lies in calculating the optimum SAR indices threshold using multi-source remote sensing data. This feature was skipped earlier in this report and will be explained in the following pages.

#### 2. Advance Flood Map Features: (Optional)

Checking the box below activates the calculation of optimum SAR index threshold values using a multi-source (SAR and Optical satellite data) calibration approach.

Calculate Optimum Thresholds

In the App environment, by checking the box next to the “Calculate Optimum Threshold” feature in the “Advance Flood Map Features” section and redrawing the boundary (as visualized in Figure 11), the App reruns and initiates the collection of available post-flood Sentinel-2 optical imagery. This collection is based on the user-defined period in the **Input Panel** for the target flood event. Then, the App starts calculating MNDWI as outlined in equation (4) to extract inundated regions using these optical images.

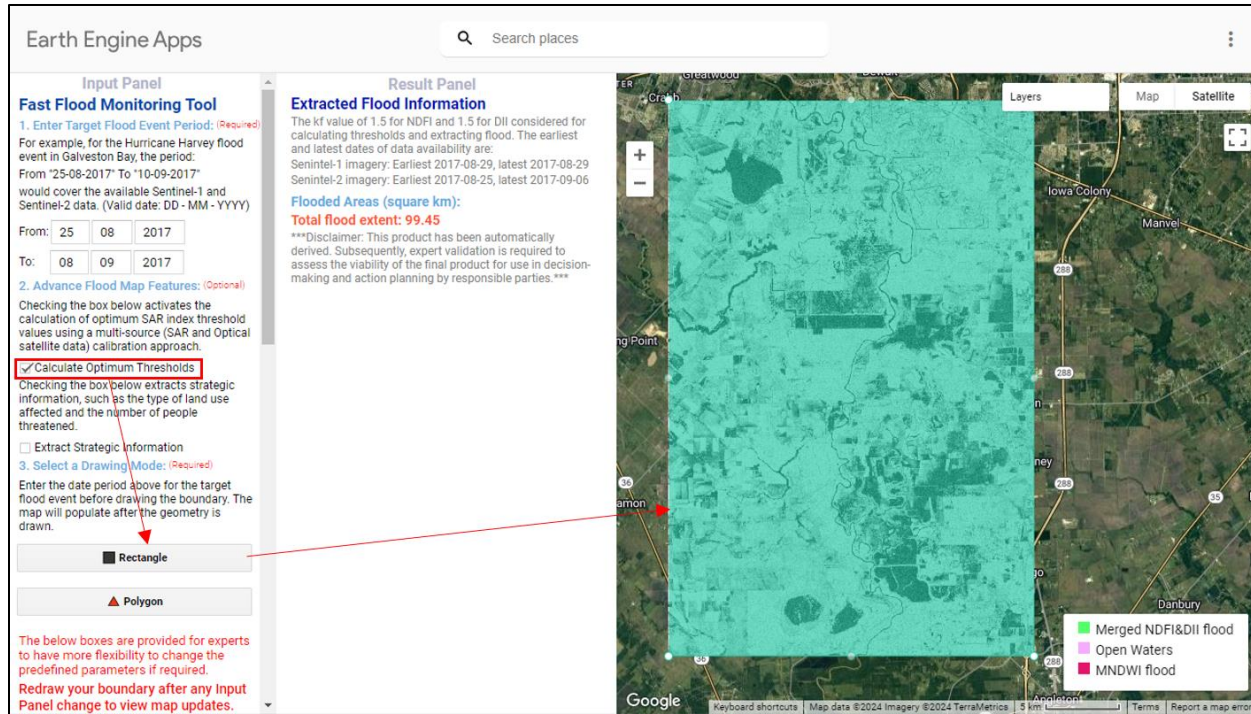


Figure 11: Activating the "Calculate Optimum Threshold" feature.

Computation time varies depending on the size of the selected study area and the accuracy of the results depends on the satellite data availability. Figure 12a presents post-flood optical images extracted by the App and Figure 12b demonstrates the corresponding flooded areas extracted using MNDWI for the Hurricane Harvey flood event in the southern region of Houston.

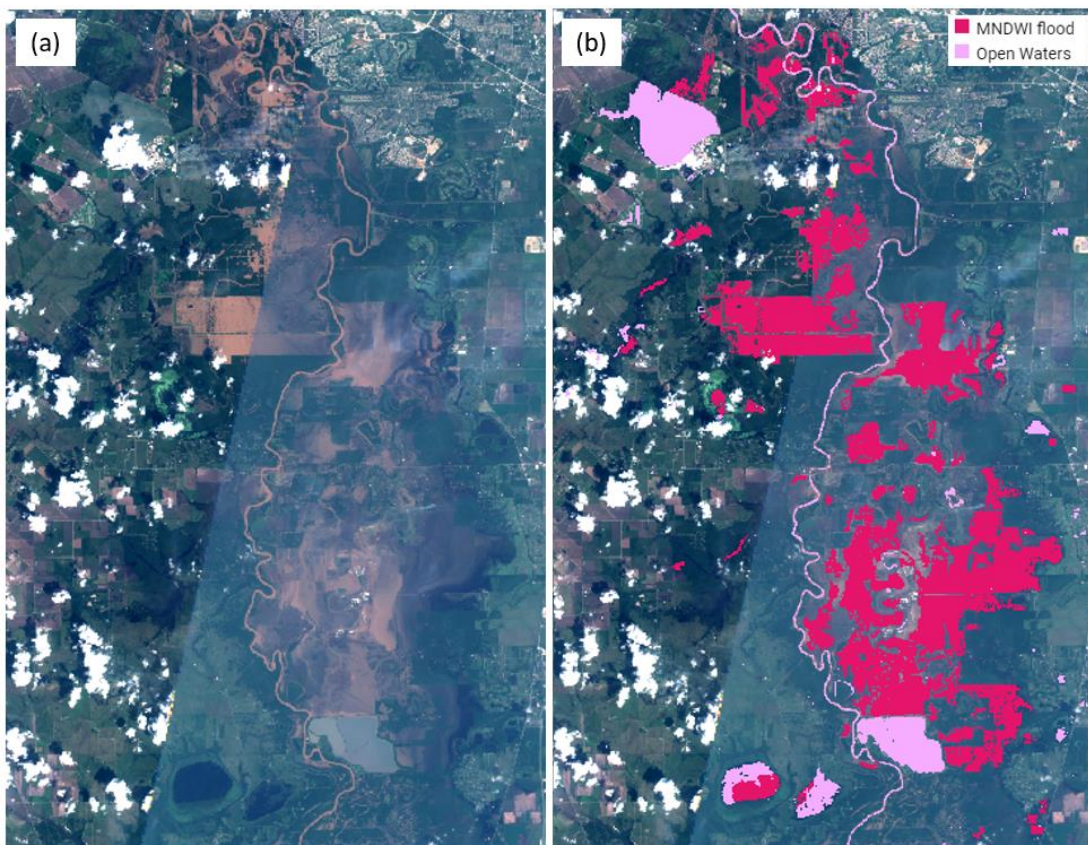


Figure 12: (a) Optical data after the Hurricane Harvey Flood and (b) extracted flood using MNDWI.

In extracting flooded pixels from the MNDWI image, the App employs a predefined threshold of 0.4. This default threshold value aligns with findings in other studies (e.g., Baig et al. [30], Phiri et al. [31], and Ferral et al. [32]) for extracting flooded pixels from the calculated MNDWI image for the Sentinel-2 dataset. For instance, Baig et al. [30] determined that a threshold of 0.41 effectively identified water in a lower basin of the Indus River [3]. While this default value facilitates rapid access to a final flood map for non-expert users, it may not be perfect threshold value for flood extraction from MNDWI images. Expert users can modify this threshold in “[IV. Adjust Threshold for MNDWI](#)” section of the **Input Panel** for more advanced flood mapping. This feature will explain later in this report.

Figure 13 overlays the two flood maps, generated from the MNDWI (Figure 12b) and the “**Combined NDFI&DII Flood**” (Figure 9), in one display, easing the comparison of differences. Figure 13 demonstrates that while flood map generated from SAR indices is effective in capturing a substantial portion of the flooded area detected by MNDWI, it still misses certain regions highlighted by this optical index.

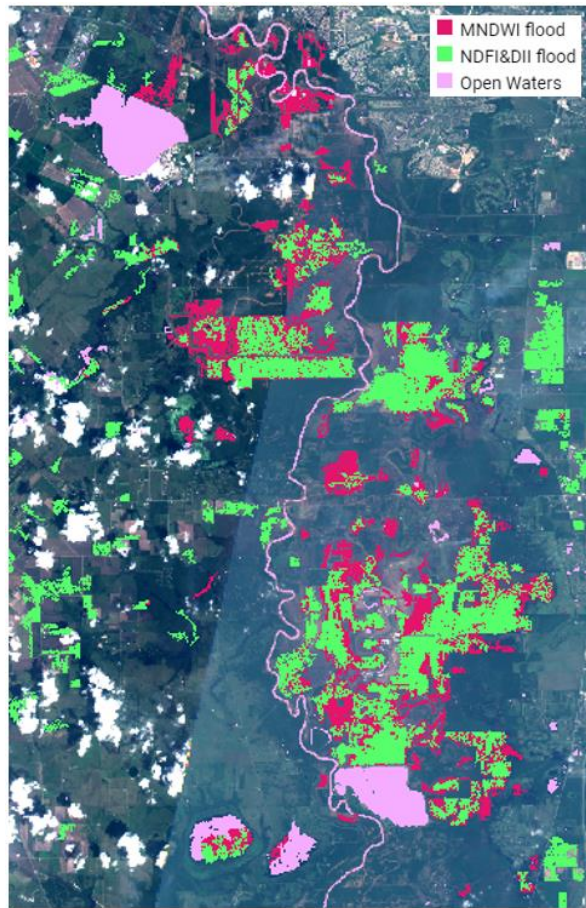


Figure 13: Comparing MNDWI and merged NDFI and DII flood extents.

To enhance the accuracy of flood extent mapping using SAR indices, expert users may adjust the  $k_f$  values for NDFI and DII in “[III. Adjust Kf Values For SAR Indices](#)” section of the **Input Panel** (will explain later) and view an updated flood map to find the best match. However, this trial-and-error process places a substantial demand on the user in terms of time and effort and does not guarantee the identification of the optimal threshold value for efficient flood extraction from SAR indices. To address this challenge, this App incorporates a sophisticated automated algorithm to calculate the optimal SAR indices threshold based on available optical data.

For sensitivity analysis, the frequency of pixel values (histograms) in each SAR index image (NDFI and DII) is examined using the threshold equation (3).  $k_f$  values are iteratively tested within a range from 0.0 to 2.0, with 0.1 increments. The flooded area extracted for each  $k_f$  value is then validated against the flood extent derived from multispectral optical imagery, utilizing the MNDWI. To evaluate the agreement ( $A_{gr}$ ) and perform sensitivity analysis assessments ( $ToA_{gr}$ ), equations (5) and (6) are utilized, respectively. The results of this sensitivity analysis on both SAR and optical flood extent maps yield optimal  $k_f$  values for SAR indices.

The formulation for calculating the agreement percentage is provided in equation (5). In this equation, B is the area where both optical and SAR indices intersect, and O presents where the optical MNDWI detects the flood [3].

$$\text{Agr \%} = \frac{B}{O} \times 100\%. \quad (5)$$

On the other hand, (7) calculates the total agreement ( $ToAgr$ ) percentage according to SAR and optical estimated flood extent. This equation is used to conduct a sensitivity analysis of flood extent maps resulting from the SAR- and Optical-based indices [3]:

$$\text{ToAgr \%} = \frac{B}{(O + Src - B)} \times 100\%. \quad (6)$$

where  $Src$  is the area of the SAR flood detections excluding the flood under cloud cover in the optical image. We exclude cloud cover from the SAR flood extent map to make it comparable with the optical image flood extent.  $B$  is subtracted from the denominator so that the intersection area is not counted twice. This effectively shows the overall difference between the SAR and optical flood detection areas where there are no clouds. In (5) and (6), a value of 100 indicates perfect agreement between SAR and optical flood area, and a value of 0 indicates the opposite.

As mentioned earlier, all the above steps will be doing in the App, by selecting the "**Calculate Optimum Threshold**" feature and redrawing the study area boundaries. So, the App will automatically start the calculation process using multi-source satellite data using SAR and optical remote sensing data. Subsequently, the  $k_f$  value associated with the highest  $ToAgr$  level with the optical flood map is identified as the optimal threshold. The optimum threshold values, along with the agreement percentage for each value, are displayed in the "**Result Panel**" under "**Updated Information**" (Figure 14). Surprisingly, the total flood extent area is almost doubled using these new threshold values (from 99.19 km<sup>2</sup> for default threshold values to 150.33 km<sup>2</sup> for optimum threshold values).

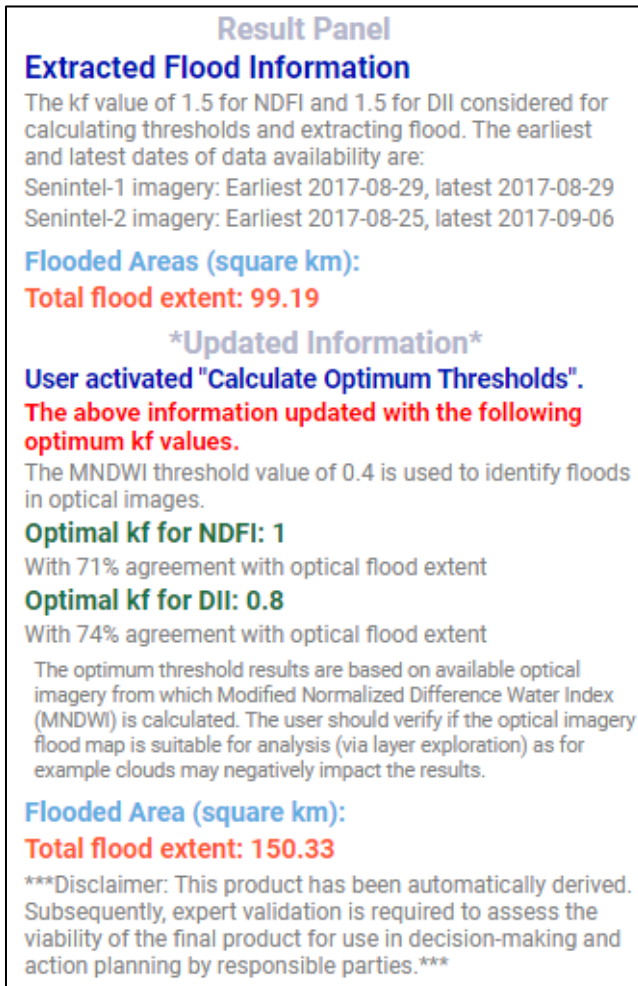


Figure 14: The updated information in the Output Panel interface.

Therefore, users can now access the updated flood map results based on the calculated optimal thresholds through the "Layers" toolbar located at the top-right corner of the interface (as indicated in Figure 7). Furthermore, Figure 15 provides a visual comparison between the optical MNDWI and the result of merging two flooded areas extracted from NDFI and DII. Figure 15a demonstrates the flood map for default  $k_f$  values, and Figure 15b shows the flood map generated using the optimal thresholds for "Combined NDFI&DII Flood" map. A comparison of these images distinctly illustrates that the updated flood map using optimum threshold values exhibits a significant improvement.

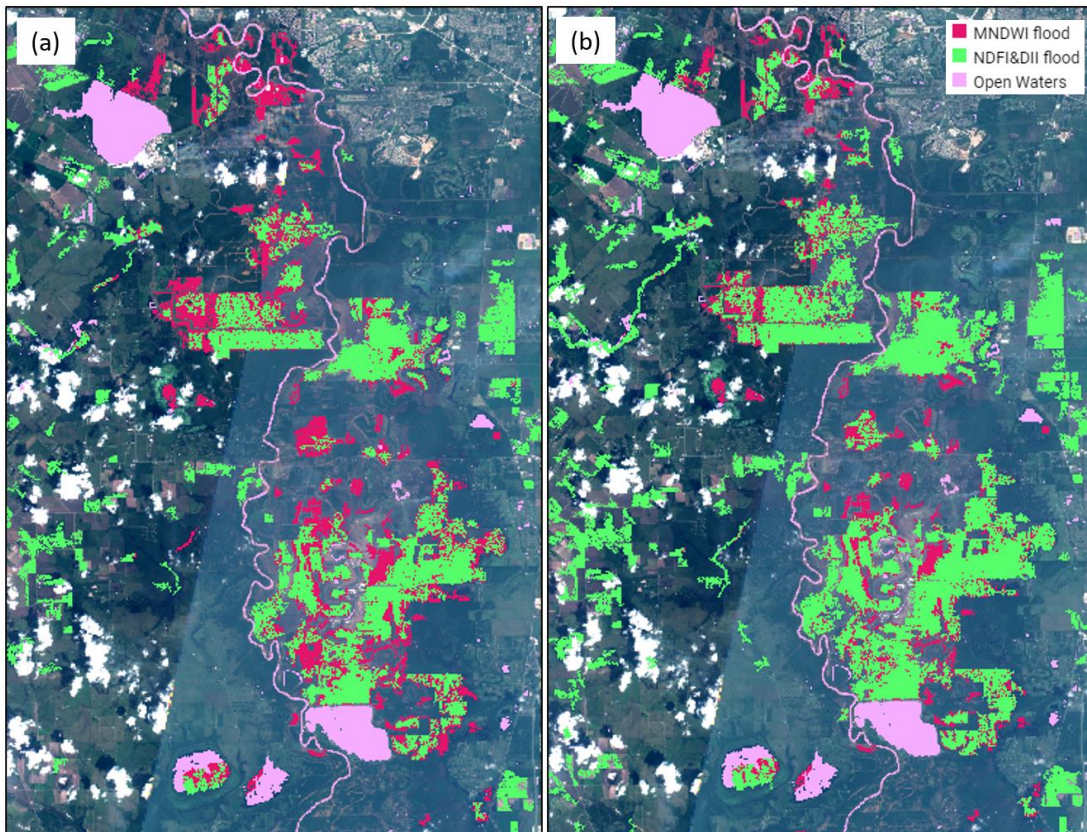


Figure 15: Comparing MNDWI and merged NDHI and DII flood extents. (a) using default threshold value and (b) using optimum threshold values.

This report demonstrates how users can utilize this App for flood monitoring and enhance the quality of the final flood map. The App's results are generated from available SAR and optical imagery that the App finds based on a user-defined time period and the location in the **Input Panel**. Expert users are advised to verify the suitability of the input images through layer exploration (see Figure 7). Additionally, it is recommended that expert knowledge is employed to review the final flood maps for decision-making and action planning by relevant parties. The following disclaimer note is included in the final App results panel:

“\*\*\*Disclaimer: This product has been automatically derived. Subsequently, expert validation is required to assess the liability of the final product for use in decision-making and action planning by responsible parties.”\*\*\*”

**Addressing Third Objective:** “Provide multidisciplinary flood hazard information for geographically strategic emergency response plans in near real-time.”

The App uses the final extracted flood extent map to estimate multidisciplinary information, such as potential damage to residential, cropland, and industrial areas. For instance, it employs Land Cover Land Used (LCLU) layers like “Global The European Space Agency (ESA) WorldCover” to estimate the extent of cropland and urban areas affected by the flood. Additionally, the App utilizes “WorldPop Global Project Population Data” to obtain high-resolution data on human population distributions, estimating the potential number of people threatened by the flood. Furthermore, “Local Climate Zones (LCZs)” datasets are used to categorize urban and

rural landscape types, estimating the amount of dense, open, and sparse building arrangements affected by the flood. These datasets enable the App to assess additional critical supplementary information from the final flood extent maps. A summary of all the datasets used is provided in Table 1.

Table 1: The datasets used in the GEE App.

Data	Source	Resolution
Sentinel-1	"COPERNICUS/S1_GRD"	10 m
Sentinel-2	"COPERNICUS/S2"	20 m
LCLU for the Globe	"ESA/WorldCover/v200"	10 m
LCLU for the USA	"USGS/NLCD_RELEASES/2019_REL/NLCD"	30 m
DEM	"NASA/NASADEM_HGT/001"	30 m
World Population	"WorldPop/GP/100m/pop"	100 m
Local Climate Zones	"RUB/RUBCLIM/LCZ/global_lczone_map/latest"	100 m
Surface Water Mapping	"JRC/GSW1_0/GlobalSurfaceWater"	30 m

Once the flood map is generated, it enables the extraction of diverse flood hazard information, contributing to strategically planned emergency response initiatives. As shown below, by checking the box "**Extract Strategic Information**" in "**Advance Flood Map Feature**" section in the **Input Panel**, the App provides more information for multidisciplinary communication from the generated flood map for decision-makers.

## 2. Advance Flood Map Features: (Optional)

Checking the box below extracts strategic information, such as the type of land use affected and the number of people threatened.

Extract Strategic Information

The extracted strategic information is displayed in the "**Result Panel**", as demonstrated in Figure 16. In this panel the source of the used datasets is provided.

### Used Datasets:

\* The resources for "Flooded Areas" information is the European Space Agency (ESA) WorldCover 10m product global land cover map. The user can change this dataset via the listbox in "II. Change LCLU dataset" section of the Input Panel.

\* The resources for "Vulnerable Area Affected" information is global map of Local Climate Zones (LCZs) at 100m pixel size for characterizing urban landscapes.

\* The resources for "Number of Population Threatened" information is WorldPop Global Project Population Data at 100m pixel size for estimating human population distributions.

If the user checks both "**Calculate Optimum Thresholds**" and "**Extract Strategic Information**" in the **Input Panel**, they can view information extracted from both the default (or user-defined)  $k_f$  value and calculated optimum  $k_f$  value in the **Results Panel**. The information is divided by the text below.

### \*Updated Information\*

User activated "**Calculate Optimum Thresholds**".

The above information updated with the following optimum kf values.

## Result Panel

### Extracted Flood Information

The  $k_f$  value of 1.5 for NDFI and 1.5 for DII considered for calculating thresholds and extracting flood. The earliest and latest dates of data availability are:  
 Senintel-1 imagery: Earliest 2017-08-29, latest 2017-08-29  
 Senintel-2 imagery: Earliest 2017-08-25, latest 2017-09-06

#### Flooded Areas (square km):

**Total flood extent: 99.08**

**Cropland flooded: 37.85**

**Urban flooded: 0.15**

#### Vulnerable Area Affected (square km):

**Heavey Industry: 0**

**Dense Arraignment Building: 0**

**Open Arraignment Building: 0**

**Sparse Arraignment Building: 5.67**

#### Number of Population Threatened:

**247 person(s)**

\*\*\*Disclaimer: This product has been automatically derived. Subsequently, expert validation is required to assess the viability of the final product for use in decision-making and action planning by responsible parties.\*\*\*

#### Used Datasets:

- \* The resources for "Flooded Areas" information is the European Space Agency (ESA) WorldCover 10m product global land cover map. The user can change this dataset via the listbox in item 3 of the Input Panel.

- \* The resources for "Vulnerable Area Affected" information is global map of Local Climate Zones (LCZs) at 100m pixel size for characterizing urban landscapes.

- \* The resources for "Number of Population Threatened" information is WorldPop Global Project Population Data at 100m pixel size for estimating human population distributions.

Figure 16: The multidisciplinary information that is shown in the **Result Panel**.

## 5- Additional Features For Expert Users

In the App input panel, after “[3. Select a Drawing Mode](#)” section, we provide the below red text to inform the user that they can leave the rest of parameter for more experts and see the flood estimation using predefined parameters.

**“The below boxes are provided for experts to have more flexibility to change the predefined parameters if required.”**

In this App, we make some assumptions to provide a fast flood map for non-expert user for delineating flood extent maps from SAR and optical satellite data. The first assumption is considering a constant  $k_f$  value of 1.5 for calculating SAR indices thresholds. This value has been used in the literature for flood mapping and it can give a fair estimation flood extent [20], [21], [27], [28], [29]. Also, a constant threshold vale of 0.4 is considered for flood pixel extraction from optical index image which aligns with findings in other studies (e.g., Baig et al. [30], Phiri et al. [31], and Ferral et al. [32]). Finally, we consider a reference time period set form “01-06-2017” to “15-06-2017”. We found that these predefined parameters are suitable for many case studies. Nevertheless, in certain instances, if some of these parameters are not adjusted, the application may be unable to generate a flood extent map. For example, if there are no images available for the predefined reference date period for the target study area, the user needs to try another reference date period. Figure 17 displays the additional features that this App provides for expert users.

**Users can view NDFI and DII Images, Flood Maps, pixel value Histograms, and analyze Affected Cropland and Urban areas.**

The user can choose between the **Globe** and **USA** dataset for extracting land cover land use information.

The user can change the default  $K_f$  values for **NDFI** and **DII**.

The user can **Download** the generated flood map.

The user can change the default **Threshold** value for **MNDWI**.

The user can change the Pre-defined **Start Date** and **End Date** of the **Refence Images**.

**Redraw your boundary after any Input Panel change to view map updates.**

**I. Display Additional Map and Graphics**

- Display NDFI and DII Flood Map Results
- Display NDFI and DII Images
- Display Histograms for NDFI and DII
- Display Cropland & Urban Affected

**II. Change LCLU dataset**

The app utilizes the European Space Agency (ESA) dataset for extracting land cover and land use information by default. If you are mapping floods for the USA, you can enhance accuracy by changing the selector list below to USA and using the United States Geological Survey (USGS) dataset.

**Globe**

**III. Adjust Kf Values For SAR Indices**

Numbers between 0.0 to 2.0 (default: 1.5). This number serves as the  $K_f$  value in the thresholding equation for extracting floods using the Normalized Difference Flood Index (NDFI) and Difference Image Index (DII) from SAR images. For more information, please refer to the following resource:

Refer to: [Hamidi et al., \(2023\)](#)

NDFI: 1.5      DII: 1.5

Get Flood Map Download Link

**IV. Adjust Threshold for MNDWI**

Numbers between 0.0 to 0.5 (default: 0.4). This number serves as the threshold for extracting floods using the Modified Normalized Difference Water Index (MNDWI) from optical images. For more information, please refer to the following resource:

Refer to: [Hamidi et al., \(2023\)](#)

MNDWI: 0.4

**V. Adjust Reference SAR Images Period**

We assigned the default reference period:  
From "01-06-2017" To "15-06-2017"  
If the default reference period does not encompass appropriate reference images within the available Sentinel-1 data, please consider adjusting the time period.

From: 01    06    2017

To: 15    06    2017

App created by Ebrahim Hamidi (University of Alabama) and reviewed by Brad G. Peter (University of Arkansas), funded by the National Science Foundation INFEWS Program and the U.S. Army Corps of Engineers. Also, partial support for development of this App is awarded.

Figure 17: The expert input panel interface of the GEE App that give more flexibility to expert users for flood extent mapping.

Furthermore, additional flexibility is provided for expert users to analyze the final flood maps and acquire more comprehensive information to ensure the reliability of the flood extent map. This includes options such as displaying the NDFI and DII images as well as the frequency distribution of these SAR index pixel values (Histograms). It should be mentioned that, if users change any parameter values or check any boxes, they need to select a drawing mode and redraw the boundary to see the updated map and information. Therefore, we provide the text below in the **Input Panel**.

**"Redraw your boundary after any Input Panel change to view map updates."**

### I. Display Additional Map and Graphics

To view the NDFI and DII flood maps before merging into the "**Combined NDFI&DII Flood**" map, check the box below. You can access these maps in the '**Layers**' toolbar located at the top-right corner of the App screen (see to Appendix I).

Display NDFI and DII Flood Map Results

To view the NDFI and DII images, check the box below. You can access these SAR index images in the '**Layers**' toolbar (see to Appendix I).

Display NDFI and DII Images

To view the frequency histograms of NDFI and DII pixel values, check the box below. The histograms will appear in the bottom-right corner of the App screen.

Display Histograms for NDFI and DII

The histograms in the App primarily serve as a visual representation of the frequency of SAR index's pixel values. While they allow experts to observe and make preliminary interpretations, it's emphasized that their primary purpose is not for the extraction of threshold values. For example, the histograms for the test case of Hurricane Harvey's flood in the south of the city of Houston are shown in Figure 18.

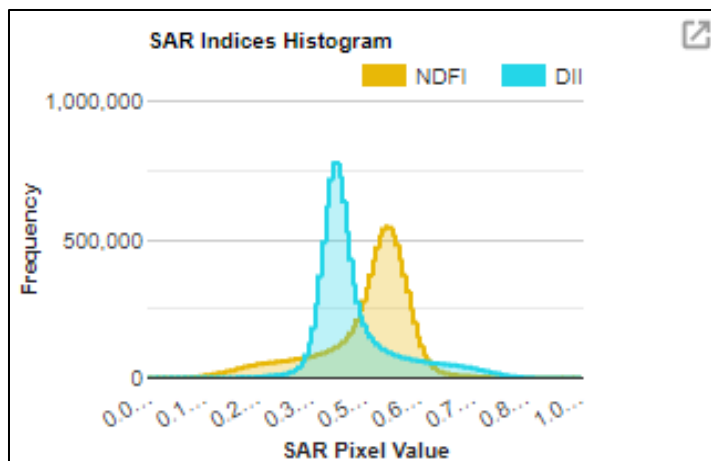


Figure 18: Histogram of pixel values from NDFI and DII.

Using the extracted flood map and the land cover land used that mentioned in Table 1, the App is able to view the map for cropland and urban area affected by flood. This feature is activated by checking the box below and the user can view the maps in the '**Layers**' toolbar.

Display Cropland & Urban Affected

### II. Change LCLU dataset

The App defaults to using the European Space Agency (ESA) dataset for extracting land cover and land use information. For enhanced accuracy in final maps of cropland and urban areas affected by flood in the USA, users can modify the selector list below to 'USA' and utilize the United States Geological Survey (USGS) dataset (refer to Table 1).



Figure 19 demonstrate the differences between using these two LCLU datasets for the USA for Hurricane Harvey's flood in the south of the city of Houston test case.

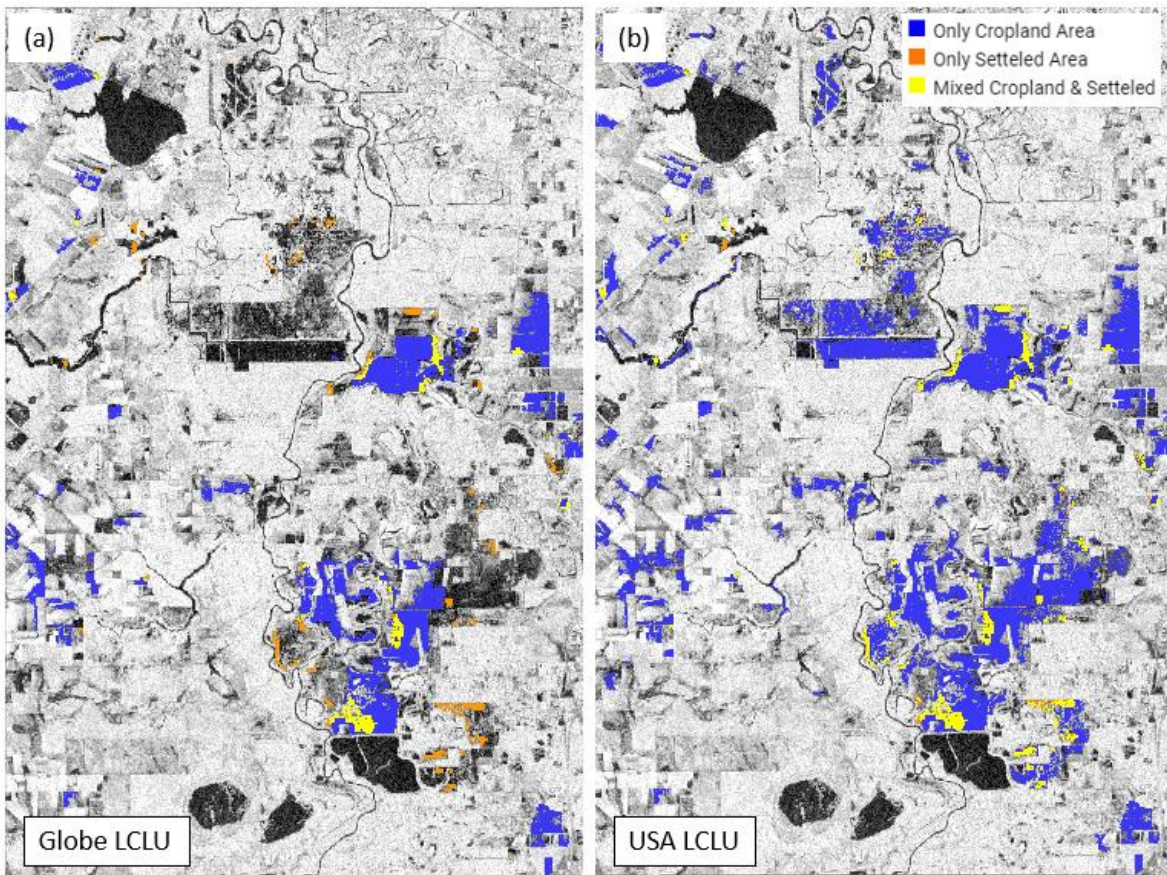


Figure 19: Classification of flooded area using (a) the European Space Agency (ESA) dataset and (b) the United States Geological Survey (USGS) dataset for Hurricane Harvey's flood in the south of the city of Houston.

### III. Adjust K<sub>f</sub> Values For SAR Indices

In this feature, the user can define a number that represents the  $k_f$  value in the thresholding equation (3) for extracting floods from the NDFI and DII images. While any number is accepted in the  $k_f$  value box, setting it within 0 to 2 times the standard deviation from the mean of the pixel value frequency histogram (equation (3)) is recommended for flooded pixel extraction. For additional details the user can refer to Hamidi et al., [3].

NDFI:  DII:

Get Flood Map Download Link

Also, checking the box next to “Get Flood Map Download Link” will provide a link for the user on the top-right of the App’s screen to download the final merged flood map for the default (or user-defined)  $k_f$  values. However, it's important to note that checking this box adds more processing time, and it is recommended to leave this box unchecked until reaching the final map.

[Click to Download Merged  
NDFI&DII Flood Map](#)

### IV. Adjust Threshold for MNDWI

In this App, a default threshold value equal to 0.4, corresponding with flooded pixels from the calculated MNDWI image for Sentinel-2 dataset, is consistent with other studies (e.g., Baig et al. [30], Phiri et al. [31], and Ferral et al. [32]). For example, Baig et al. [30] found that a threshold of 0.41 worked for identifying water in a lower basin of the Indus River [3]. Considering these default values can help non-expert users access a rapid final flood map. While it may not be perfect, it could be useful for urgent flood mitigations. Although any

number is accepted in the MNDWI box as a threshold value, we suggest considering a number between 0.0 to 0.5 (default: 0.4) to examine the flooded areas from optical images. For additional details, the user can refer to Hamidi et al. [13].

MNDWI:

## V. Adjust Reference SAR Images Period

The App preassigned date considered for the reference date period, form “01-06-2017” to “15-06-2017”.

**From:**     
**To:**

If the default reference period does not encompass appropriate SAR reference images within the available Sentinel-1 data, the user can examine other date periods in the provided boxes using the "DD - MM - YYYY" format. For instance, there might be no images available for the predefined reference date period for the target study area; if so, the user needs to try another reference date period.

## 6- Research Challenges and Limitations

The development of this App encountered challenges right from the outset, and each step presented its own set of difficulties, requiring more time than initially anticipated. While numerous challenges have been addressed in the final version of the App, this section highlights some additional challenges and limitations.

While we acknowledge the advantages of utilizing Sentinel-2 images to enhance the accuracy of the final flood map, we are aware of the inherent challenges associated with optical images. These challenges include potential errors in classifying cloud shadows as water and difficulty in mapping floods beneath vegetation, canopies, and debris accumulations [8]. Additionally, the MNDWI-based floodwater delineation method relies on setting a threshold value, which introduces the possibility of underestimating or overestimating flood extents, a common concern with thresholding techniques.

SAR imaging, on the other hand, is not without its challenges, including misclassification of tarmac surfaces as water, missing floodwater during windy and rainy conditions, and difficulties in detecting floods under vegetation and in densely built-up areas due to double-bounce backscattering signatures [20]. Furthermore, discrepancies between optical and SAR flooded areas can occur, leading to an increased error percentage, particularly when using different image resolutions, variable acquisition times, and diverse flood extent detection techniques [20], [21], [33].

The temporal resolution of the data is another consideration, as it may miss the unpredictable dynamics of flood events and fail to capture floods during critical conditions. To address these challenges, we emphasize the importance of employing complementary techniques and data sources, aiming for daily or higher temporal resolution information for effective flood emergency management. The utilization of multiple images and ground-truth data, such as high watermark collections, can contribute to reducing uncertainties in validating flood extents.

The App's speed has emerged as a challenge, and we addressed it by optimizing the code, eliminating redundancies, and improving the efficiency of the application. This effort is critical for flood monitoring at larger scales and improving the user experience. Nonetheless, for calibration procedures that require iterations to find the best thresholds, the computation time varies depending on the size of the selected study area. Therefore, if the user applies this optimization for a large study area, it may take a significant amount of time to obtain the optimum threshold values, or there is a possibility that the App fails to reach the final optimum values results. On the other hand, the accuracy of the results highly depends on the availability of satellite data. For instance, cloud shadows in the optical data could be considered as flooded areas, contributing to inaccurate optimum threshold values.

It should be mentioned that the accuracy of demographic and multidisciplinary information relies on the datasets used in the App, as specified in Table 1. Unexpected flood information could result from inappropriate spatial resolution or the date of data collection in the datasets.

## 7- Links Ror the App's Code and Dissemination Documents

The automated code, App, and final report is available to the community in a documented, discoverable repository uploaded on CUAHSI's HydroShare, and GitHub and they are accessible throughout the following links:

**GitHub link:**

<https://github.com/ebrahimhamidi/FastFloodMonitoringTool-FFMT>

**CUAHSI Hydroshare:**

[Fast Flood Monitoring Tool - FFMT | CUAHSI HydroShare](#)

Hamidi, E., B. Peter (2024). Fast Flood Monitoring Tool - FFMT, HydroShare,  
<http://www.hydroshare.org/resource/bf66a6cc204d4691abda18833bf68760>

Also, here are the code and App environment in the Google Earth Engine App:

**The App link:**

<https://turnkey-aleph-386916.projects.earthengine.app/view/geefastfloodmonitoring>

**The App code:**

<https://code.earthengine.google.com/cbfc0e96562cc79f75407cf1c48ebf93>

## 8- Acknowledgement:

This App has undergone a review by Dr. Brad Peter, whose insightful comments, suggestions, and expertise have been instrumental in the development of this valuable flood-mapping tool. I am sincerely grateful for his unwavering support and patience throughout the app's creation. I would also like to express my appreciation to CUAHSI for their enthusiasm for advancing water science within the community. Their support throughout the Hydroinformatics Innovative Fellowship (HIF) has been a driving force behind the realization of this tool.

The acknowledgment below is displayed on the **Input Panel** to recognize all the organizations involved in funding this project.

App created by Ebrahim Hamidi (University of Alabama) and reviewed by Brad G. Peter (University of Arkansas), funded by the National Science Foundation INFEWS Program and the U.S. Army Corps of Engineers. Also, partial support for development of this App is awarded through CUAHSI's 2023 Hydroinformatics Innovation Fellowship (HIF).

## 9- Test Case Examples:

In this section, the App is tested through specific examples, highlighting its diverse features. First, the assumed inputs and the location of the area under study are presented. Following that, resulting maps and extracted information from the targeted flood event are provided, offering a detailed exploration of the application's capabilities.

### Example 1: The flood event on February 2023 in south of Mozambique, Africa.

#### 1. Enter Target Flood Event Period (Required)

**From:** 12 – 02 – 2023

**To:** 14 – 02 – 2023

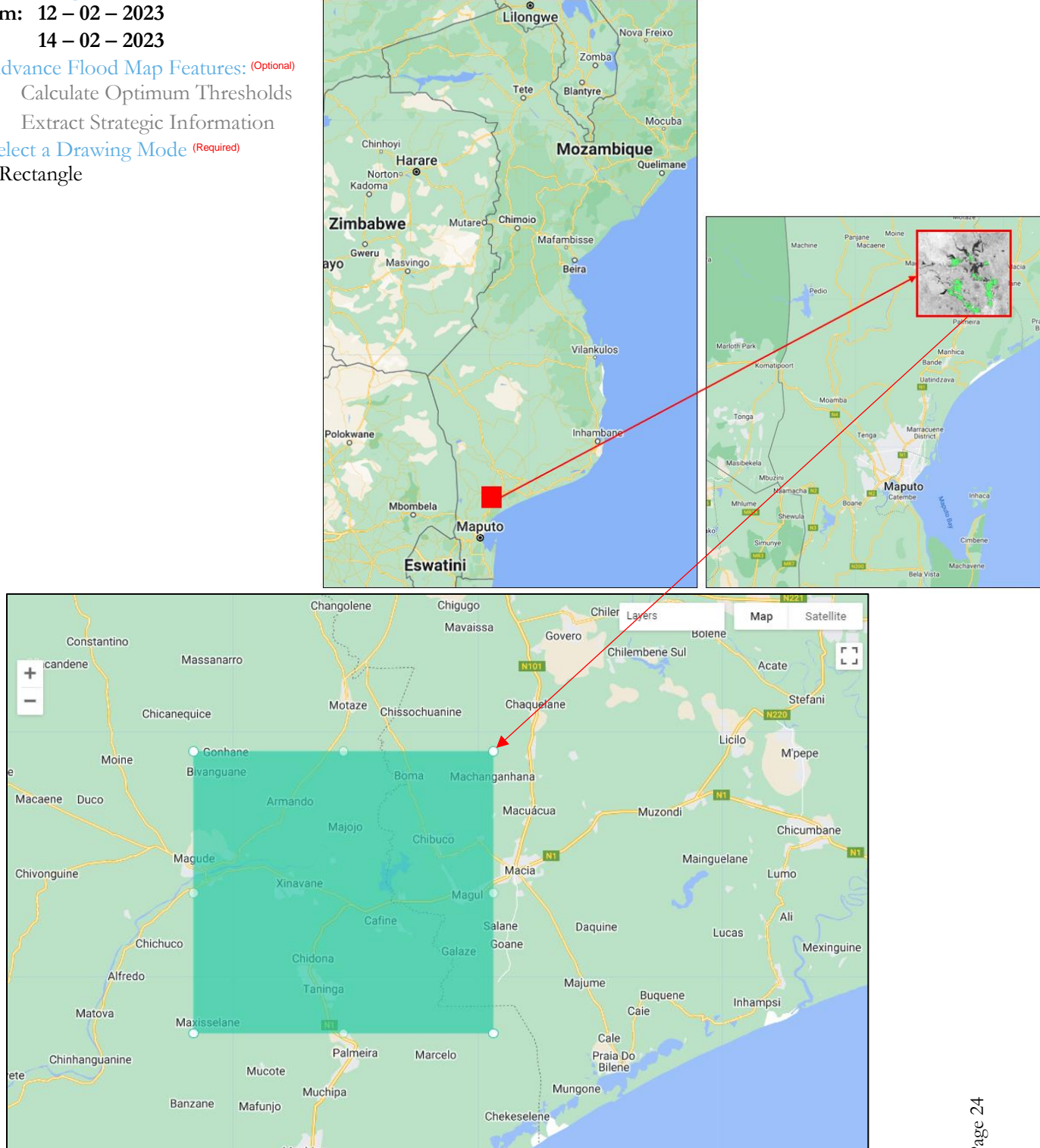
#### 2. Advance Flood Map Features: (Optional)

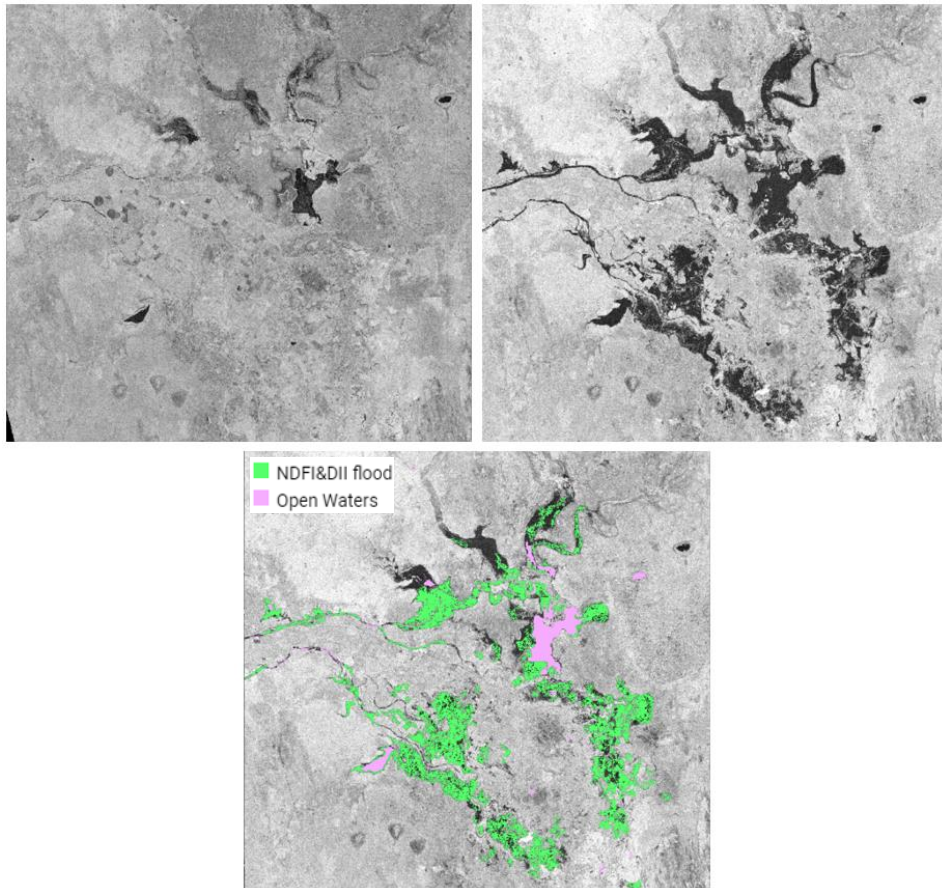
Calculate Optimum Thresholds

Extract Strategic Information

#### 3. Select a Drawing Mode (Required)

Rectangle





### Result Panel

#### Extracted Flood Information

The kf value of 1.5 for NDFI and 1.5 for DII considered for calculating thresholds and extracting flood. The earliest and latest dates of data availability are:

Sentinel-1 imagery: Earliest 2023-02-13, latest 2023-02-13

Sentinel-2 imagery: Earliest 2023-02-12, latest 2023-02-12

#### Flooded Areas (square km):

**Total flood extent: 113.06**

**Cropland flooded: 32.83**

**Urban flooded: 0.012**

#### Vulnerable Area Affected (square km):

**Heavy Industry: 0**

**Dense Arraignment Building: 0**

**Open Arraignment Building: 0**

**Sparse Arraignment Building: 0**

#### Number of Population Threatened:

**3403 person(s)**

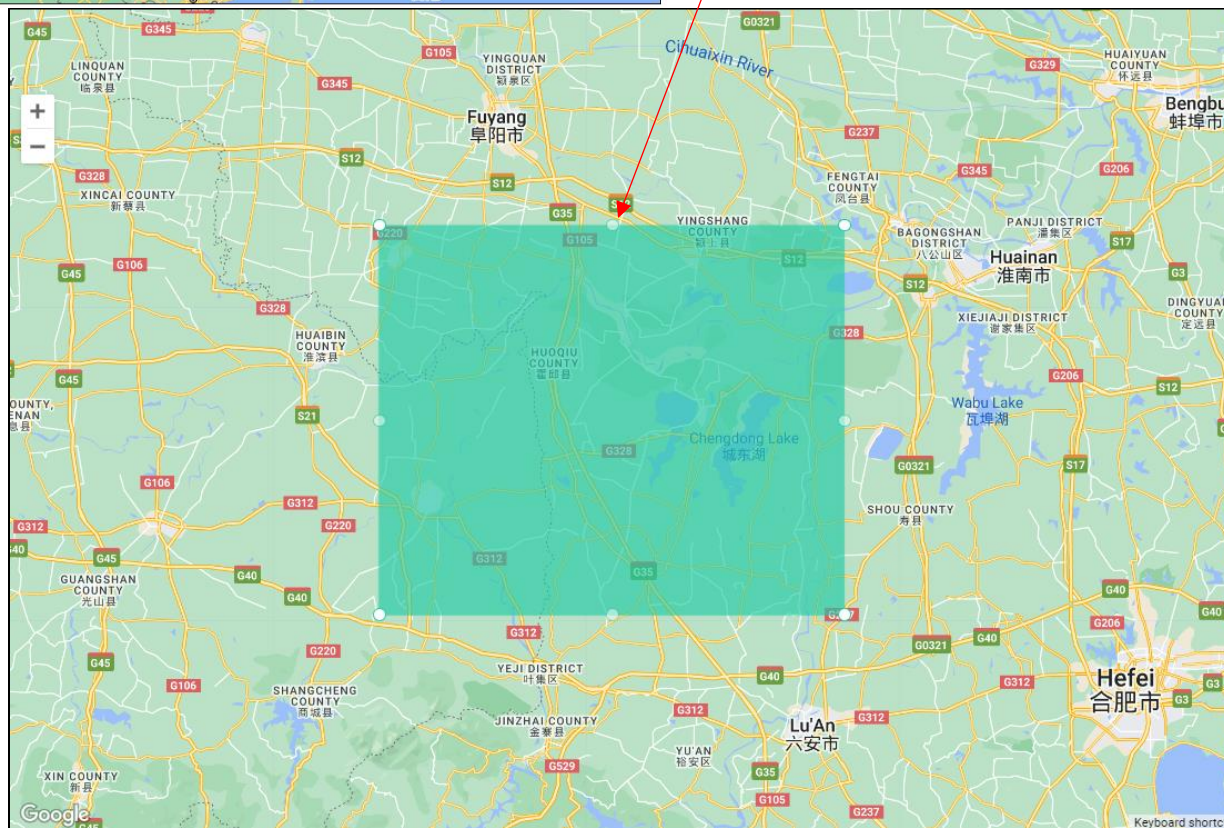
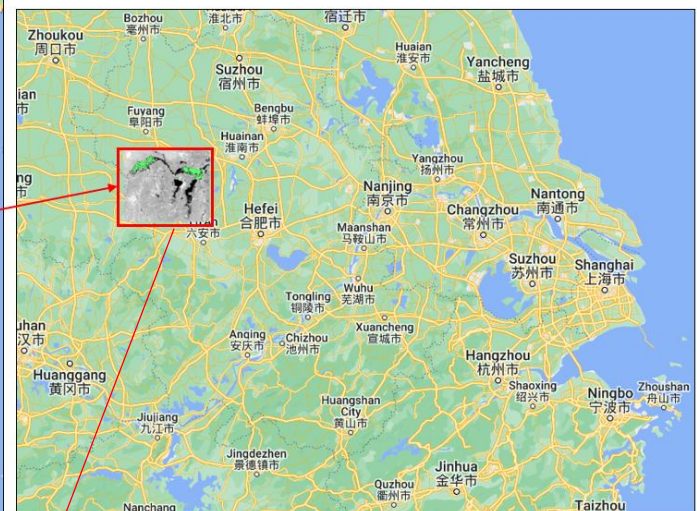
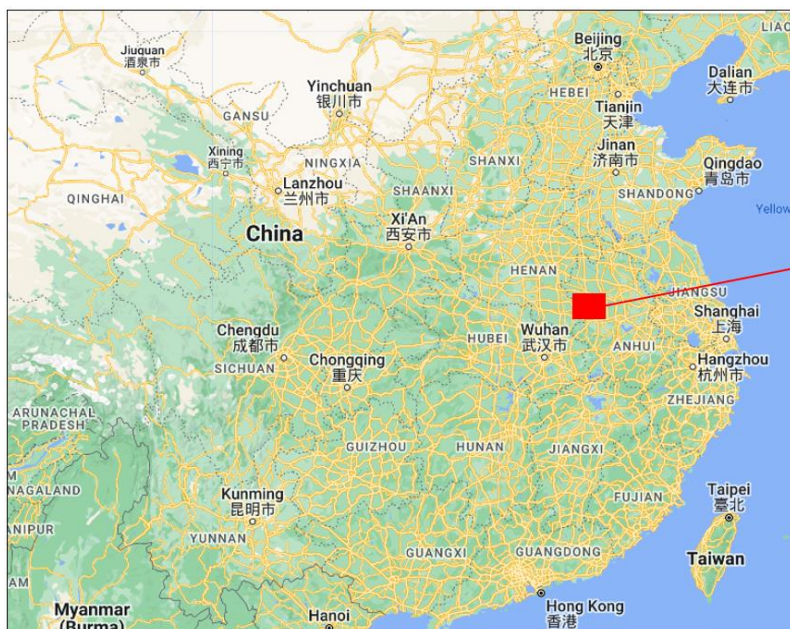
\*\*\*Disclaimer: This product has been automatically derived. Subsequently, expert validation is required to assess the viability of the final product for use in decision-making and action planning by responsible parties.\*\*\*

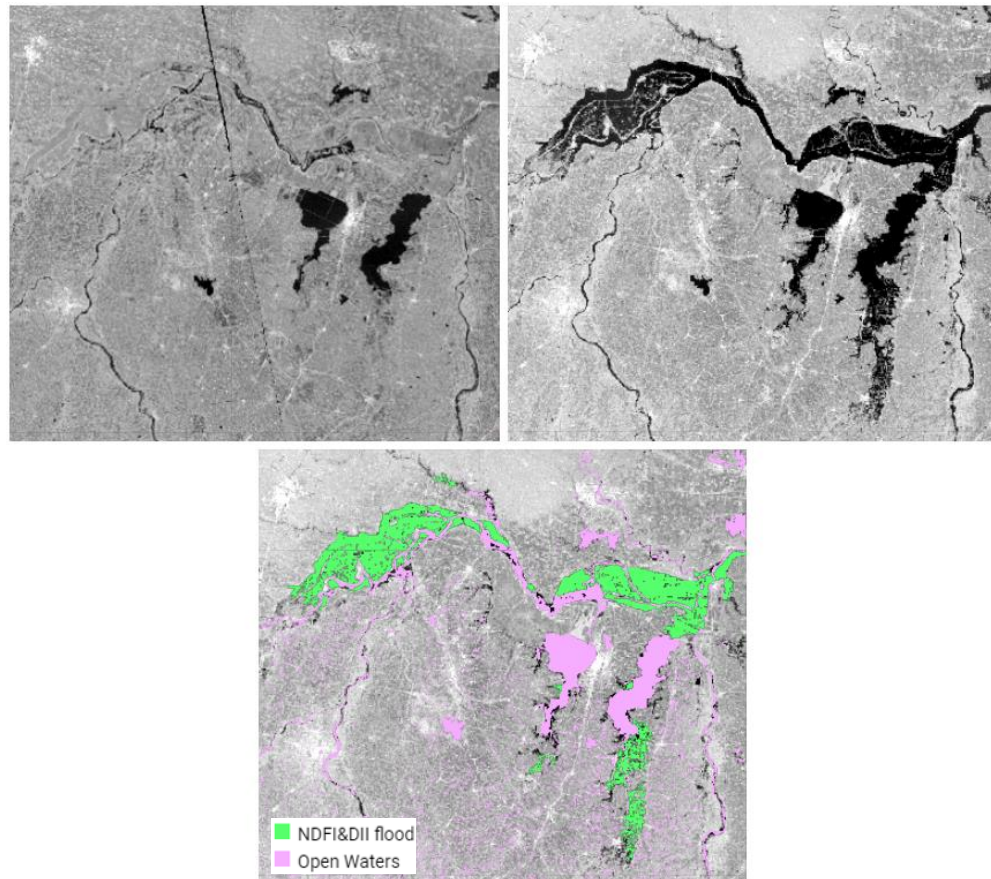
#### Used Datasets:

\* The resources for "Flooded Areas" information is the European Space Agency (ESA) WorldCover 10m product global land cover map. The user can change this dataset via the listbox in item 3 of the Input Panel.

\* The resources for "Vulnerable Area Affected" information is global map of Local Climate Zones (LCZs) at 100m pixel size for characterizing urban landscapes.

\* The resources for "Number of Population Threatened" information is WorldPop Global Project Population Data at 100m pixel size for estimating human population distributions.

**Example 2: The flood event on August 2020, west of China.****1. Enter Target Flood Event Period (Required)****From:** 01 – 08 – 2020**To:** 05 – 08 – 2020**2. Advance Flood Map Features: (Optional)** Calculate Optimum Thresholds Extract Strategic Information**3. Select a Drawing Mode (Required)** Rectangle



**Result Panel**

### Extracted Flood Information

The kf value of 1.5 for NDFI and 1.5 for DII considered for calculating thresholds and extracting flood. The earliest and latest dates of data availability are:

- Sentinel-1 imagery: Earliest 2020-08-01, latest 2020-08-01
- Sentinel-2 imagery: Earliest 2020-08-02, latest 2020-08-04

**Flooded Areas (square km):**

- Total flood extent: 678.02
- Cropland flooded: 609.47
- Urban flooded: 1.707

**Vulnerable Area Affected (square km):**

- Heavy Industry: 0
- Dense Arraignment Building: 0
- Open Arraignment Building: 0
- Sparse Arraignment Building: 0

**Number of Population Threatened:**

163010 person(s)

\*\*\*Disclaimer: This product has been automatically derived. Subsequently, expert validation is required to assess the viability of the final product for use in decision-making and action planning by responsible parties.\*\*\*

**Used Datasets:**

- \* The resources for "Flooded Areas" information is the European Space Agency (ESA) WorldCover 10m product global land cover map. The user can change this dataset via the listbox in item 3 of the Input Panel.
- \* The resources for "Vulnerable Area Affected" information is global map of Local Climate Zones (LCZs) at 100m pixel size for characterizing urban landscapes.
- \* The resources for "Number of Population Threatened" information is WorldPop Global Project Population Data at 100m pixel size for estimating human population distributions.

**Example 3: The flood event on August-September 2022 after Hurricane Ian, Florida, USA.**

**1. Enter Target Flood Event Period (Required)**

**From:** 28 – 09 – 2022

**To:** 05 – 10 – 2022

**2. Advance Flood Map Features: (Optional)**

Calculate Optimum Thresholds

Extract Strategic Information

**3. Select a Drawing Mode (Required)**

Rectangle

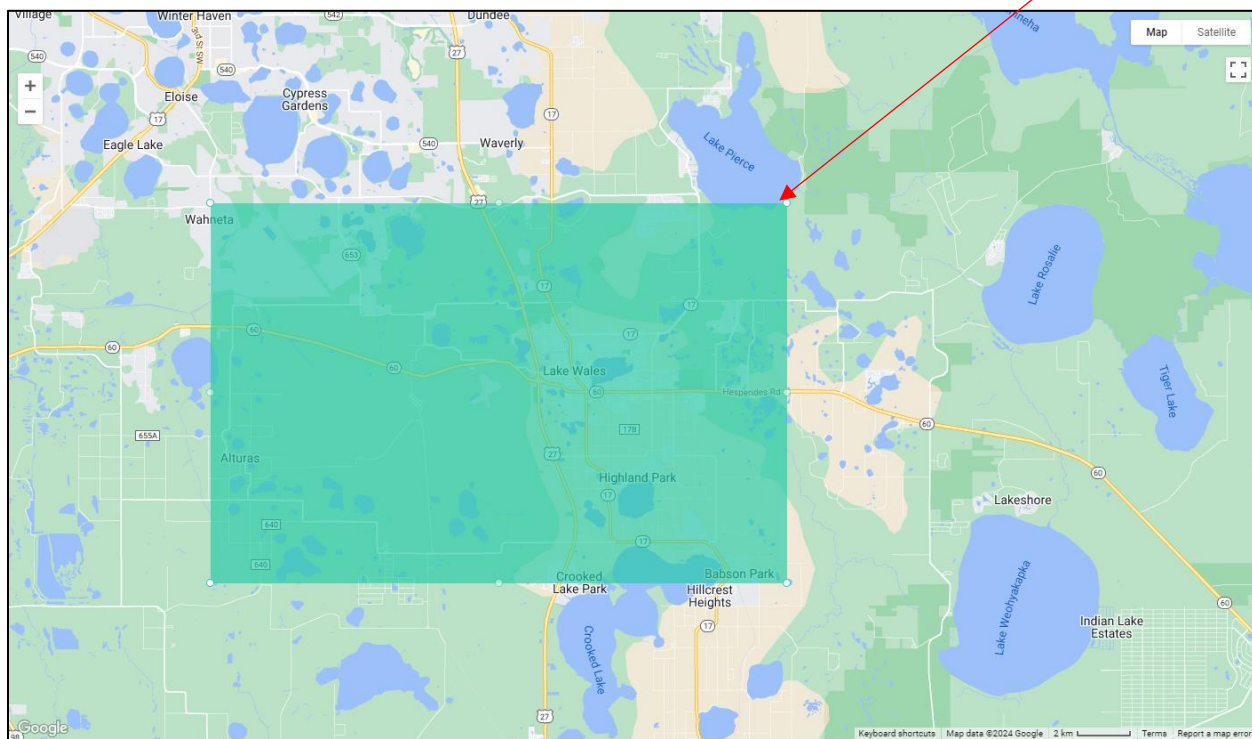
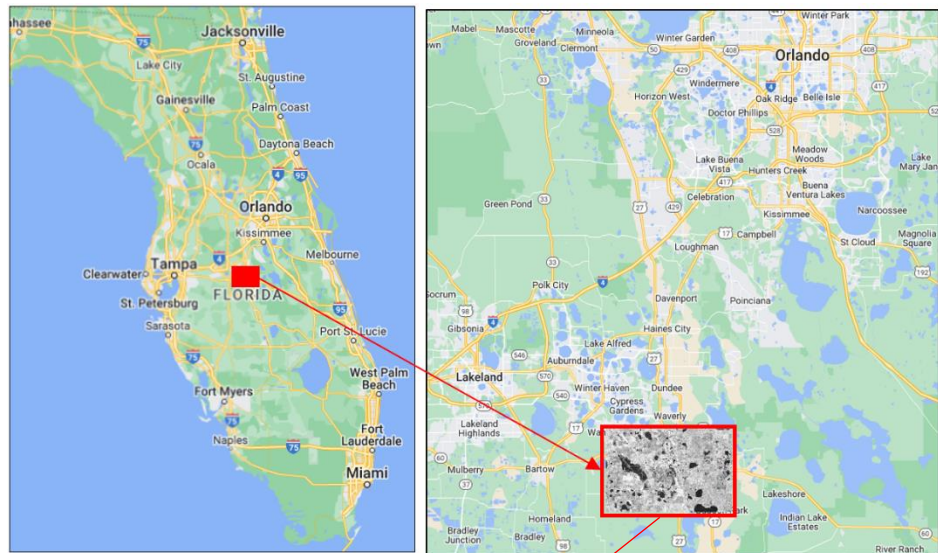
**IV. Adjust Threshold for MNDWI**

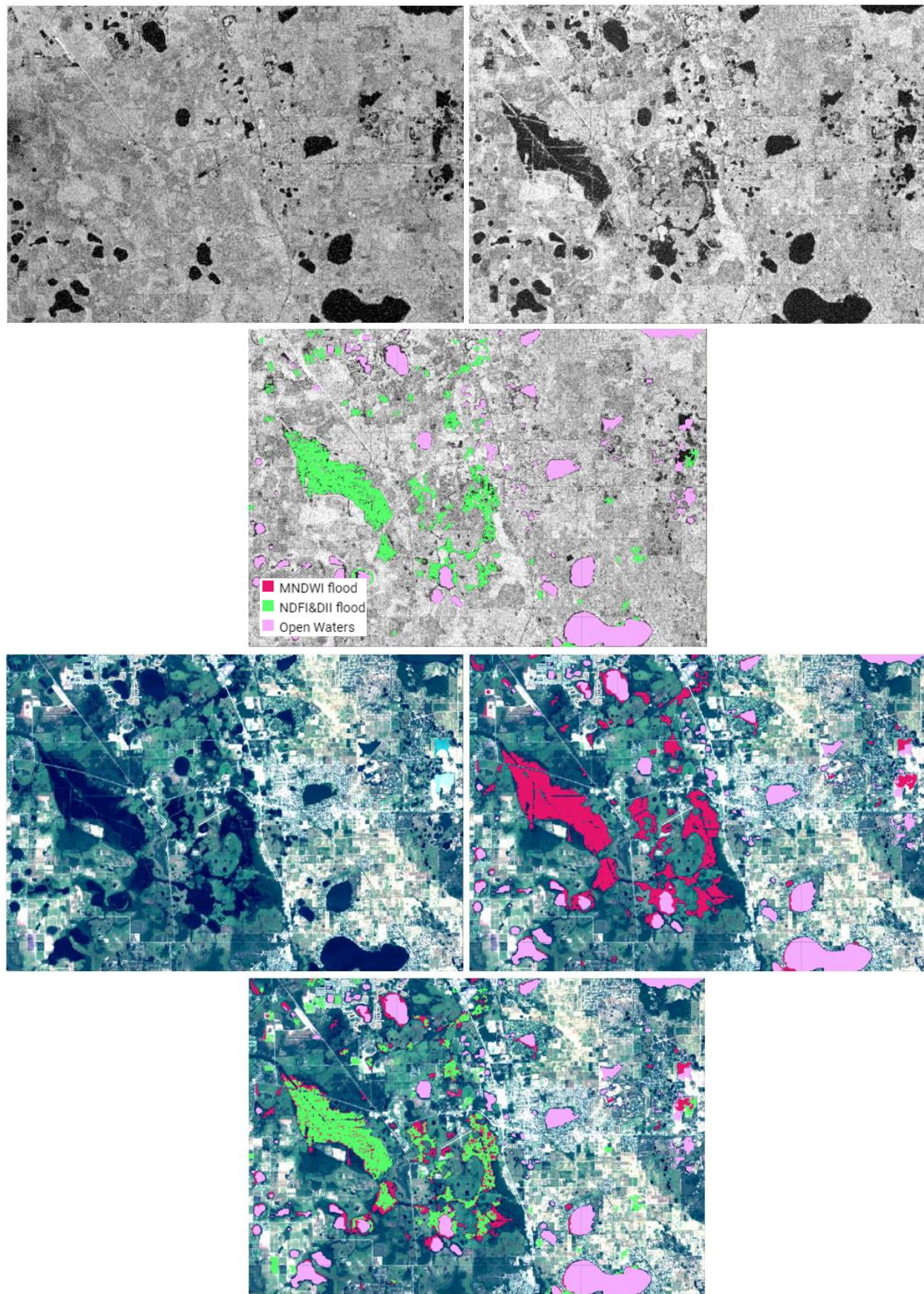
MNDWI: 0.05

**V. Adjust Reference SAR Images Period**

**From:** 01 - 06 - 2018

**To:** 15 – 06 - 2018





## Result Panel

### Extracted Flood Information

The kf value of 1.5 for NDFI and 1.5 for DII considered for calculating thresholds and extracting flood. The earliest and latest dates of data availability are:

Senintel-1 imagery: Earliest 2022-10-02, latest 2022-10-02

Senintel-2 imagery: Earliest 2022-09-30, latest 2022-09-30

#### Flooded Areas (square km):

**Total flood extent: 17.7**

**Cropland flooded: 0.65**

**Urban flooded: 0.037**

#### Vulnerable Area Affected (square km):

**Heavey Industry: 0**

**Dense Arraignment Building: 0**

**Open Arraignment Building: 0.01**

**Sparse Arraignment Building: 0.32**

#### Number of Population Threatened:

**25 person(s)**

\*Updated Information\*

User activated "Calculate Optimum Thresholds".

The above information updated with the following optimum kf values.

The MNDWI threshold value of 0.05 is used to identify floods in optical images.

**Optimal kf for NDFI: 1.4**

With 67% agreement with optical flood extent

**Optimal kf for DII: 1.4**

With 66% agreement with optical flood extent

The optimum threshold results are based on available optical imagery from which Modified Normalized Difference Water Index (MNDWI) is calculated. The user should verify if the optical imagery flood map is suitable for analysis (via layer exploration) as for example clouds may negatively impact the results.

#### Flooded Area (square km):

**Total flood extent: 19.1**

**Croplands flooded: 0.7**

**Urban flooded: 0.059**

#### Vulnerable Area Affected (square km):

**Heavey Industry: 0**

**Dense Arraignment Building: 0**

**Open Arraignment Building: 0.01**

**Sparse Arraignment Building: 0.41**

#### Number of Population Threatened:

**29 person(s)**

\*\*\*Disclaimer: This product has been automatically derived.

Subsequently, expert validation is required to assess the

viability of the final product for use in decision-making and

action planning by responsible parties.\*\*\*

**Example 3: The flood event on September 2018 after Hurricane Florence, North Carolina, USA.**

**1. Enter Target Flood Event Period (Required)**

From: 15 – 09 – 2018

To: 20 – 09 – 2018

**2. Advance Flood Map Features: (Optional)**

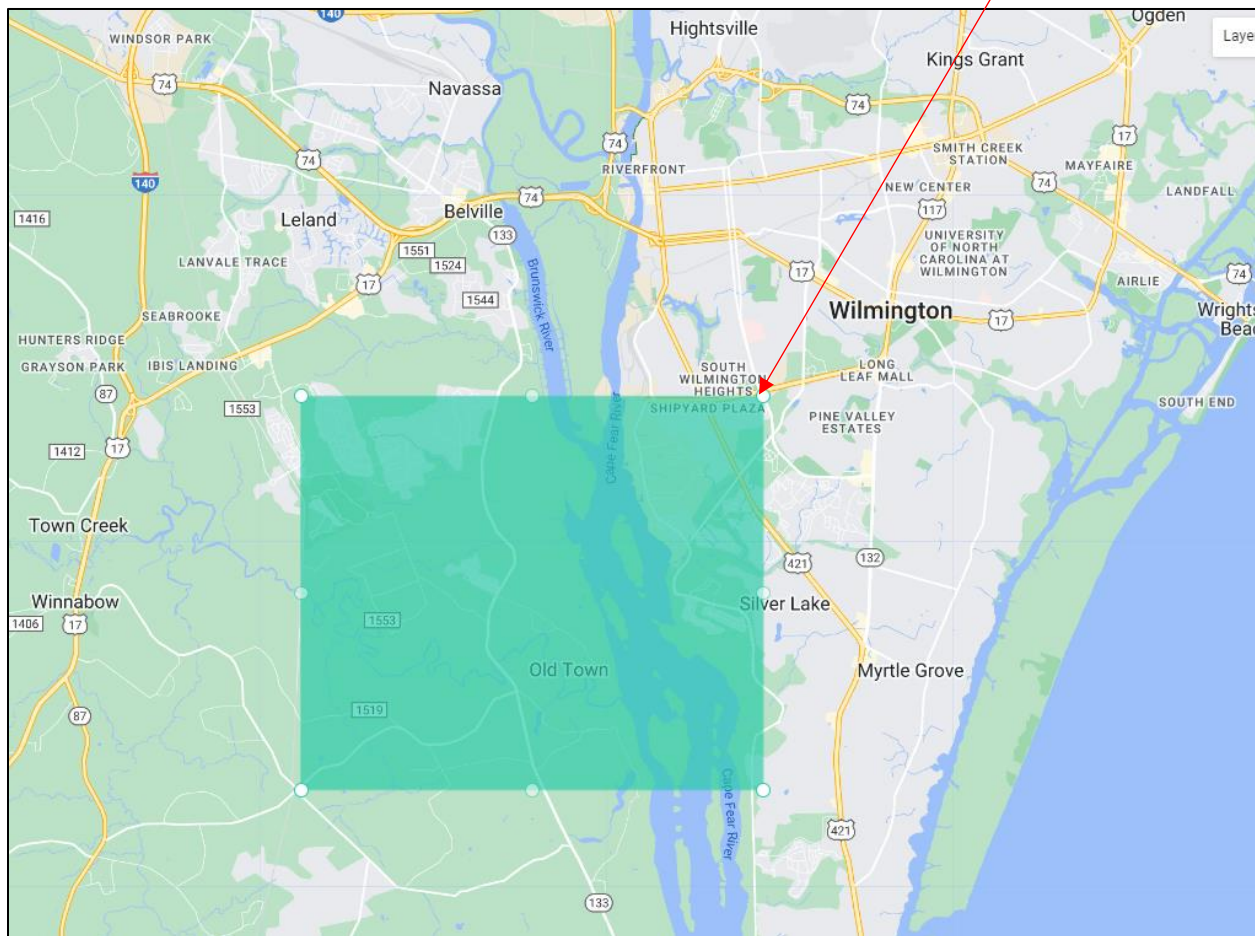
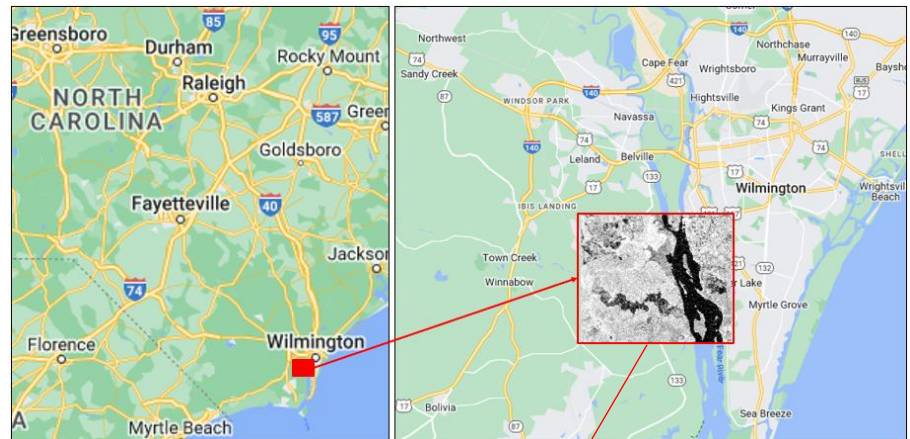
- Calculate Optimum Thresholds
- Extract Strategic Information

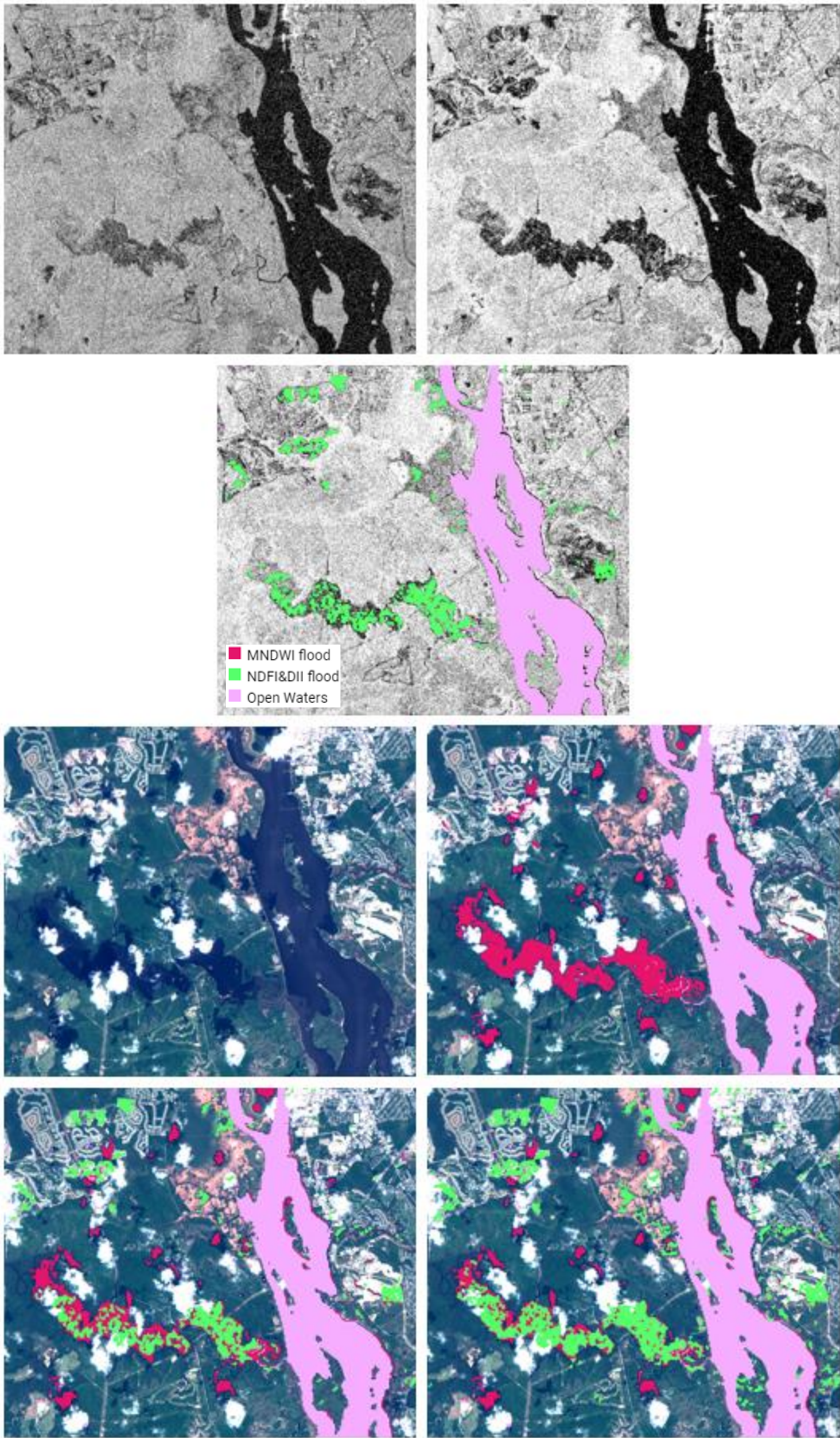
**3. Select a Drawing Mode (Required)**

- Rectangle

**IV. Adjust Threshold for MNDWI**

MNDWI: 0.20





## Result Panel

### Extracted Flood Information

The kf value of 1.5 for NDFI and 1.5 for DII considered for calculating thresholds and extracting flood. The earliest and latest dates of data availability are:

Senintel-1 imagery: Earliest 2018-09-19, latest 2018-09-19

Senintel-2 imagery: Earliest 2018-09-18, latest 2018-09-18

#### Flooded Areas (square km):

**Total flood extent: 4.35**

**Cropland flooded: 0**

**Urban flooded: 0.224**

#### Vulnerable Area Affected (square km):

**Heavey Industry: 0**

**Dense Arraignment Building: 0**

**Open Arraignment Building: 0**

**Sparse Arraignment Building: 0.16**

#### Number of Population Threatened:

**8 person(s)**

\*Updated Information\*

User activated "Calculate Optimum Thresholds".

The above information updated with the following optimum kf values.

The MNDWI threshold value of 0.2 is used to identify floods in optical images.

**Optimal kf for NDFI: 1**

With 52% agreement with optical flood extent

**Optimal kf for DII: 0.8**

With 54% agreement with optical flood extent

The optimum threshold results are based on available optical imagery from which Modified Normalized Difference Water Index (MNDWI) is calculated. The user should verify if the optical imagery flood map is suitable for analysis (via layer exploration) as for example clouds may negatively impact the results.

#### Flooded Area (square km):

**Total flood extent: 7.55**

**Croplands flooded: 0.03**

**Urban flooded: 0.402**

#### Vulnerable Area Affected (square km):

**Heavey Industry: 0**

**Dense Arraignment Building: 0**

**Open Arraignment Building: 0.17**

**Sparse Arraignment Building: 0.43**

#### Number of Population Threatened:

**24 person(s)**

\*\*\*Disclaimer: This product has been automatically derived.

Subsequently, expert validation is required to assess the viability of the final product for use in decision-making and action planning by responsible parties.\*\*\*

## 10- References:

- [1] OECD, *Financial Management of Flood Risk*. OECD, 2016. doi: 10.1787/9789264257689-en.
- [2] R. Sadiq, M. Imran, and F. Oflı, "Remote Sensing for Flood Mapping and Monitoring," in *International Handbook of Disaster Research*, A. Singh, Ed., Singapore: Springer Nature Singapore, 2023, pp. 679–697. doi: 10.1007/978-981-19-8388-7\_178.
- [3] E. Hamidi, B. G. Peter, D. F. Munoz, H. Moftakhari, and H. Moradkhani, "Fast Flood Extent Monitoring with SAR Change Detection Using Google Earth Engine," *IEEE Trans. Geosci. Remote Sensing*, pp. 1–1, 2023, doi: 10.1109/TGRS.2023.3240097.
- [4] M. Taherkhani, S. Vitousek, P. L. Barnard, N. Frazer, T. R. Anderson, and C. H. Fletcher, "Sea-level rise exponentially increases coastal flood frequency," *Sci Rep*, vol. 10, no. 1, p. 6466, Dec. 2020, doi: 10.1038/s41598-020-62188-4.
- [5] H. Moftakhari, J. E. Schubert, A. Aghakouchak, R. A. Matthew, and B. F. Sanders, "Linking statistical and hydrodynamic modeling for compound flood hazard assessment in tidal channels and estuaries," *Advances in Water Resources*, vol. 128, pp. 28–38, Jun. 2019, doi: 10.1016/j.advwatres.2019.04.009.
- [6] M. E. Hamidi, M. R. Hashemi, N. Talebbeydokhti, and S. P. Neill, "Numerical modelling of the mild slope equation using localised differential quadrature method," *Ocean Engineering*, vol. 47, pp. 88–103, Jun. 2012, doi: 10.1016/j.oceaneng.2012.03.004.
- [7] A. Aghakouchak *et al.*, "Climate Extremes and Compound Hazards in a Warming World," *Annu. Rev. Earth Planet. Sci.*, vol. 48, no. 1, pp. 519–548, May 2020, doi: 10.1146/annurev-earth-071719-055228.
- [8] D. Munasinghe, S. Cohen, Y.-F. Huang, Y.-P. Tsang, J. Zhang, and Z. Fang, "Intercomparison of Satellite Remote Sensing-Based Flood Inundation Mapping Techniques," *J Am Water Resour Assoc*, vol. 54, no. 4, pp. 834–846, Aug. 2018, doi: 10.1111/1752-1688.12626.
- [9] I. Shustikova, A. Domeneghetti, J. C. Neal, P. Bates, and A. Castellarin, "Comparing 2D capabilities of HEC-RAS and LISFLOOD-FP on complex topography," *Hydrological Sciences Journal*, vol. 64, no. 14, pp. 1769–1782, Oct. 2019, doi: 10.1080/02626667.2019.1671982.
- [10] X. Zhang, C. E. Jones, T. Oliver-Cabrera, M. Simard, and S. Fagherazzi, "Using rapid repeat SAR interferometry to improve hydrodynamic models of flood propagation in coastal wetlands," *Advances in Water Resources*, vol. 159, p. 104088, Jan. 2022, doi: 10.1016/j.advwatres.2021.104088.
- [11] D. Notti, D. Giordan, F. Caló, A. Pepe, F. Zucca, and J. Galve, "Potential and Limitations of Open Satellite Data for Flood Mapping," *Remote Sensing*, vol. 10, no. 11, p. 1673, Oct. 2018, doi: 10.3390/rs10111673.
- [12] D. C. Mason, R. Speck, B. Devereux, G. J.-P. Schumann, J. C. Neal, and P. D. Bates, "Flood Detection in Urban Areas Using TerraSAR-X," *IEEE Trans. Geosci. Remote Sensing*, vol. 48, no. 2, pp. 882–894, Feb. 2010, doi: 10.1109/TGRS.2009.2029236.
- [13] B. Brisco, N. Short, J. van der Sanden, R. Landry, and D. Raymond, "A semi-automated tool for surface water mapping with RADARSAT-1," *null*, vol. 35, no. 4, pp. 336–344, Jan. 2009, doi: 10.5589/m09-025.
- [14] X. Tong *et al.*, "An approach for flood monitoring by the combined use of Landsat 8 optical imagery and COSMO-SkyMed radar imagery," *ISPRS Journal of Photogrammetry and Remote Sensing*, vol. 136, pp. 144–153, Feb. 2018, doi: 10.1016/j.isprsjprs.2017.11.006.
- [15] X. Chen, J. Li, Y. Zhang, and L. Tao, "CHANGE DETECTION WITH MULTI-SOURCE DEFECTIVE REMOTE SENSING IMAGES BASED ON EVIDENTIAL FUSION," *ISPRS Ann. Photogramm. Remote Sens. Spatial Inf. Sci.*, vol. III-7, pp. 125–132, Jun. 2016, doi: 10.5194/isprsaannals-III-7-125-2016.
- [16] X. Shan *et al.*, "Using Multidisciplinary Analysis to Develop Adaptation Options against Extreme Coastal Floods," *Int J Disaster Risk Sci*, vol. 13, no. 4, pp. 577–591, Aug. 2022, doi: 10.1007/s13753-022-00421-6.
- [17] V. S. K. Vanama, Y. S. Rao, and C. M. Bhatt, "Change detection based flood mapping using multi-temporal Earth Observation satellite images: 2018 flood event of Kerala, India," *European Journal of Remote Sensing*, vol. 54, no. 1, pp. 42–58, Jan. 2021, doi: 10.1080/22797254.2020.1867901.
- [18] B. DeVries, C. Huang, J. Armston, W. Huang, J. W. Jones, and M. W. Lang, "Rapid and robust monitoring of flood events using Sentinel-1 and Landsat data on the Google Earth Engine," *Remote Sensing of Environment*, vol. 240, p. 111664, Apr. 2020, doi: 10.1016/j.rse.2020.111664.
- [19] D. Amitrano, G. Di Martino, A. Iodice, D. Riccio, and G. Ruella, "Unsupervised Rapid Flood Mapping Using Sentinel-1 GRD SAR Images," *IEEE Trans. Geosci. Remote Sensing*, vol. 56, no. 6, pp. 3290–3299, Jun. 2018, doi: 10.1109/TGRS.2018.2797536.
- [20] M. A. Clement, C. G. Kilsby, and P. Moore, "Multi-temporal synthetic aperture radar flood mapping using change detection: Multi-temporal SAR flood mapping using change detection," *J Flood Risk Management*, vol. 11, no. 2, pp. 152–168, Jun. 2018, doi: 10.1111/jfr3.12303.
- [21] S. Long, T. E. Fatoyinbo, and F. Policelli, "Flood extent mapping for Namibia using change detection and thresholding with SAR," *Environ. Res. Lett.*, vol. 9, no. 3, p. 035002, Mar. 2014, doi: 10.1088/1748-9326/9/3/035002.
- [22] J. Lu, J. Li, G. Chen, L. Zhao, B. Xiong, and G. Kuang, "Improving Pixel-Based Change Detection Accuracy Using an Object-Based Approach in Multitemporal SAR Flood Images," *IEEE J. Sel. Top. Appl. Earth Observations Remote Sensing*, vol. 8, no. 7, pp. 3486–3496, Jul. 2015, doi: 10.1109/JSTARS.2015.2416635.
- [23] G. Nico, M. Pappalepore, G. Pasquarello, A. Rerice, and S. Samarelli, "Comparison of SAR amplitude vs. coherence flood detection methods - a GIS application," *International Journal of Remote Sensing*, vol. 21, no. 8, pp. 1619–1631, Jan. 2000, doi: 10.1080/014311600209931.
- [24] S. Schlaffer, M. Chini, L. Giustarini, and P. Matgen, "Probabilistic mapping of flood-induced backscatter changes in SAR time series," *International Journal of Applied Earth Observation and Geoinformation*, vol. 56, pp. 77–87, Apr. 2017, doi: 10.1016/j.jag.2016.12.003.
- [25] S. Cohen *et al.*, "Sensitivity of Remote Sensing Floodwater Depth Calculation to Boundary Filtering and Digital Elevation Model Selections," *Remote Sensing*, vol. 14, no. 21, p. 5313, Oct. 2022, doi: 10.3390/rs14215313.
- [26] L. L. Hess, J. M. Melack, and D. S. Simonett, "Radar detection of flooding beneath the forest canopy: a review," *International Journal of Remote Sensing*, vol. 11, no. 7, pp. 1313–1325, Jul. 1990, doi: 10.1080/01431169008955095.
- [27] F. Cian, M. Marconcini, and P. Ceccato, "Normalized Difference Flood Index for rapid flood mapping: Taking advantage of EO big data," *Remote Sensing of Environment*, vol. 209, pp. 712–730, May 2018, doi: 10.1016/j.rse.2018.03.006.
- [28] M. Singha *et al.*, "Identifying floods and flood-affected paddy rice fields in Bangladesh based on Sentinel-1 imagery and Google Earth Engine," *ISPRS Journal of Photogrammetry and Remote Sensing*, vol. 166, pp. 278–293, Aug. 2020, doi: 10.1016/j.isprsjprs.2020.06.011.
- [29] W. Wu, W. Wang, M. E. Meadows, X. Yao, and W. Peng, "Cloud-based typhoon-derived paddy rice flooding and lodging detection using multi-temporal Sentinel-1&2," *Front. Earth Sci.*, vol. 13, no. 4, pp. 682–694, Dec. 2019, doi: 10.1007/s11707-019-0803-7.
- [30] M. H. A. Baig, L. Zhang, S. Wang, G. Jiang, S. Lu, and Q. Tong, "COmparison of MNDWI and DFI for water mapping in flooding season," in *2013 IEEE International Geoscience and Remote Sensing Symposium - IGARSS*, Melbourne, Australia: IEEE, Jul. 2013, pp. 2876–2879. doi: 10.1109/IGARSS.2013.6723425.
- [31] D. Phiri, M. Simwanda, and V. Nyirenda, "Mapping the impacts of cyclone Idai in Mozambique using Sentinel-2 and OBIA approach," *South African Geographical Journal*, vol. 103, no. 2, pp. 237–258, Apr. 2021, doi: 10.1080/03736245.2020.1740104.
- [32] A. Ferral, E. Luccini, A. Aleksinkó, and C. M. Scavuzzo, "Flooded-area satellite monitoring within a Ramsar wetland Nature Reserve in Argentina," *Remote Sensing Applications: Society and Environment*, vol. 15, p. 100230, Aug. 2019, doi: 10.1016/j.rsase.2019.04.003.
- [33] L. Yan and D. P. Roy, "Improved time series land cover classification by missing-observation-adaptive nonlinear dimensionality reduction," *Remote Sensing of Environment*, vol. 158, pp. 478–491, Mar. 2015, doi: 10.1016/j.rse.2014.11.024.

## Appendix I: More Detail on Flood Extraction From SAR Index Images

This App used a change detection method for extracting flooded pixels from SAR data. For Change detection methods we need images before and after flood as shown in Figure I.

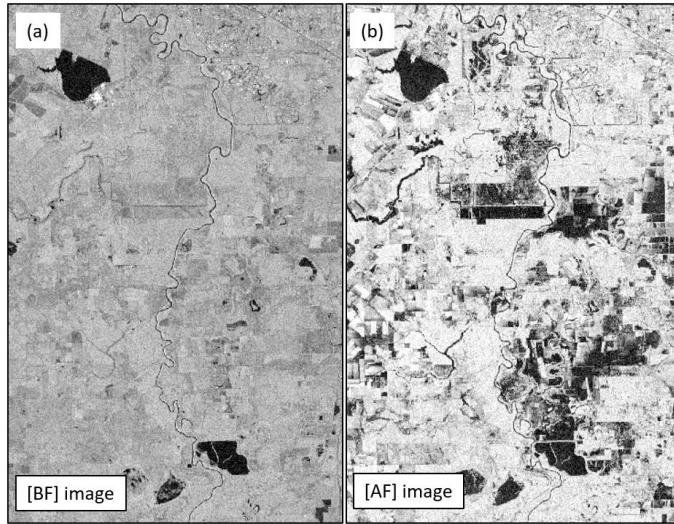


Figure I: SAR data (a) mean pixel values from pre-flood SAR Images, and (b) minimum pixel values from post-flood SAR Images.

So, by having before and after images, we can apply a change detection approach for flood mapping. This App uses the Normalized Difference Flood Index (NDFI) and Difference Image Index (DII) as change detection SAR index for flood delineation. The NDFI and DII are calculated using equations (1) and (2), respectively. In these equations,  $\sigma_0_{[BF]}$  and  $\sigma_0_{[AF]}$  are the backscatter coefficient of SAR imagery before (Figure Ia) and after (Figure Ib) the flood, respectively [3], [21], [27].

$$NDFI = \frac{|mean(\sigma_0_{[BF]})| - |min(\sigma_0_{[AF]})|}{|mean(\sigma_0_{[BF]})| + |min(\sigma_0_{[AF]})|} \quad (1)$$

$$DII = |min(\sigma_0_{[AF]})| - |mean(\sigma_0_{[BF]})| \quad (2)$$

Then the calculated NDFI and DII images are normalized to a 0-1 scale. Figures IIa and IIb show the results normalized NDFI and DII images, respectively. The user can view these images by checking the box next to “**Display NDFI and DII Images**” in the “**I. Display Additional Map and Graphics**” section of the **Input Panel**.

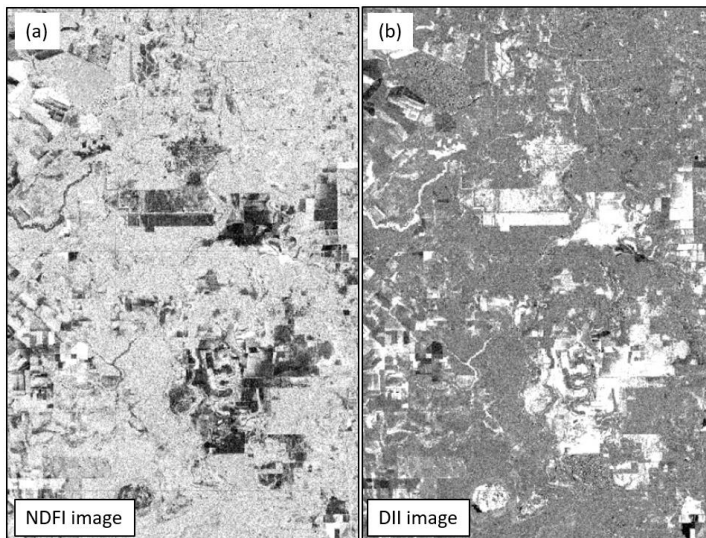


Figure II: The Normalized (a) NDFI image and (b) DII image.

It is evident that the NDFI and DII images (Figures IIa and IIb) clearly highlight the changes when comparing before and after the flood images (Figures Ia and Ib). To extract flooded pixels using these SAR index images, this App uses below equation (equation (3)) for calculating threshold values.

$$Thr = \text{mean}(SAR\ Index\ Image) \pm k_f \times \text{stdev}(SAR\ Index\ Image)$$

where the threshold value ( $Thr$ ) is determined using ( $k_f$ ) standard deviations from the mean of the SAR index image as described in equation (3).

Once the App has NDFI and DII images ready, it can easily calculate the mean and standard deviation of these SAR index images in equation (3). Only the  $k_f$  value remains unknown in this equation. Several studies in the literature have suggested using a threshold of 1.5 as a reliable value for identifying flooded pixels in SAR index images [20], [21], [27], [28], [29].

So, the App uses the default value of 1.5 for the  $k_f$  coefficient in equation (3) to calculate threshold values and extract flooded pixels from SAR index images. This default value can be changed in the “[III. Adjust Kf Values For SAR Indices](#)” section of the **Input Panel**.

In this Threshold formulation, a negative sign is applied for NDFI, classifying pixel values below the threshold as representing flooded areas. Conversely, for DII in equation (3), a positive sign is used, categorizing pixel values exceeding the threshold as depicting flooded regions. You can see the results of extracted pixels in Figure III.

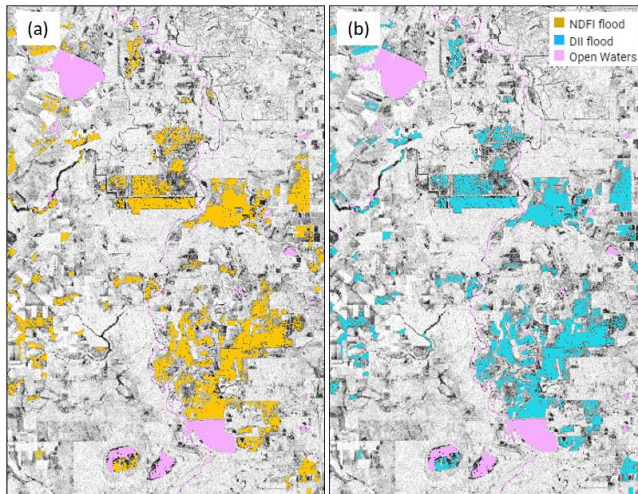


Figure III: Extracted flood pixels from (a) NDFI and (b) DII indices images.

Then, the App merges the two flooded areas extracted from NDFI and DII indices in order to decrease the chance of missing flooded pixels (i.e., reducing errors of omission). Figure IV depicts the result of merged layers.



Figure IV: Result of merging two flooded areas extracted from NDFI and DII.

## **Appendix II: Poster Presentation at The AGU 2023 Fall Meeting**

The results of this research study were presented at the 2023 American Geophysical Union (AGU) Fall Meeting. The poster can be viewed on the AGU iPoster Session below, and it is also attached to this file.

Online AGU iPoster Session:

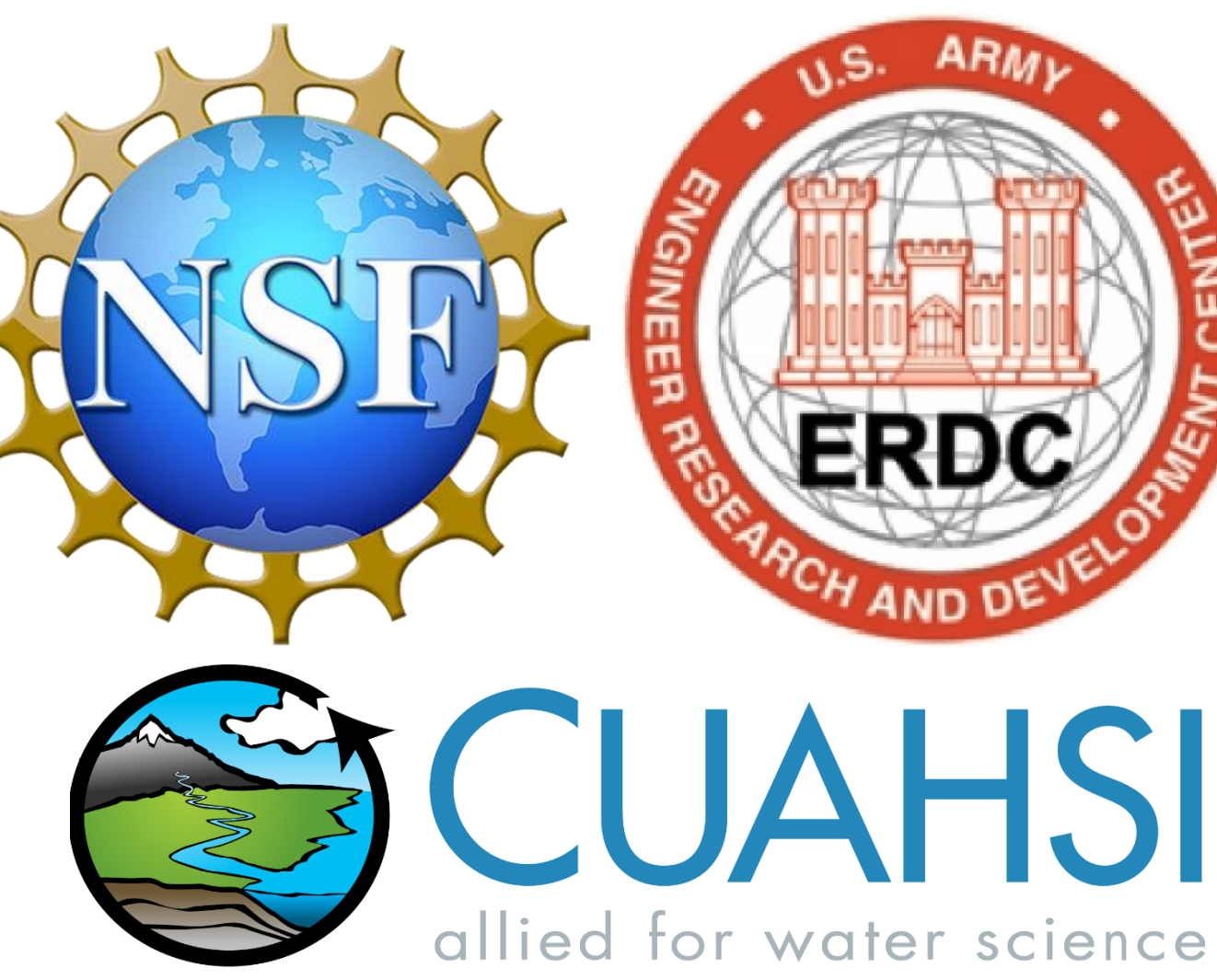
<https://agu23.ipostersessions.com/default.aspx?s=E7-71-4E-4C-43-75-A1-3B-9B-6B-97-5E-83-D0-99-C1>



# H31Y-1839: A Google Earth Engine App for Urgent Flood Mapping

Ebrahim Hamidi (shamidi1@crimson.ua.edu)<sup>1,2</sup>, Brad G. Peter<sup>3</sup>, Hamed Moftakhar<sup>1,2</sup> and Hamid Moradkhani<sup>1,2</sup>

1) Department of Civil, Construction and Environmental Engineering, The University of Alabama; 2) Center for Complex Hydroystems Research, The University of Alabama; 3) Department of Geosciences, The University of Arkansas.



## ABSTRACT

Recent studies suggest that global warming will lead to a greater chance of extreme flooding in the coming decades. Remotely sensed observations have provided researchers with decades of continuous and reliable data for extracting flood information. However, satellite revisit cycles, spatial resolution, weather conditions, and solar reflectance dependency, as well as sensor defects, are a number of remote sensing limitations that can hinder flood mapping progress. Multi-source methods can address part of the limitations inherent in single-source methods. In this study, we build on our previous research and introduce an app that leverages state-of-the-art remote sensing resources and the capability of the Google Earth Engine (GEE) platform to produce a rapid estimation of floods using an advanced multi-source remote sensing approach that is geographically generalizable. This GEE App extracts multidisciplinary information from the final flood map for responsible responders to adopt flexible measures based on the types of land-use and land-cover affected.

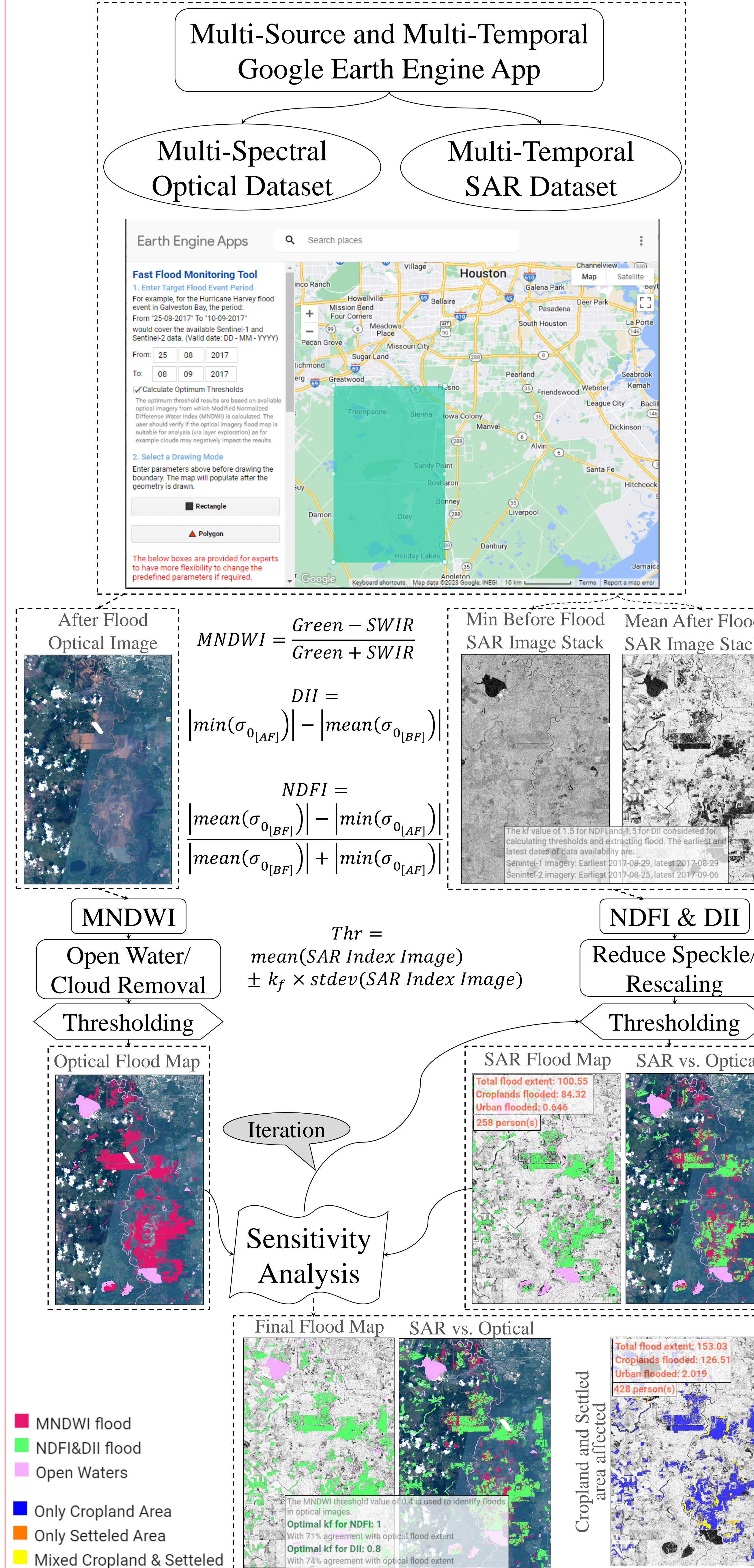
## BACKGROUND

Coastal regions are highly vulnerable to flooding due to various drivers such as extreme rainfall and tropical cyclones. Therefore, identifying efficient and accurate models for mapping floods is key in flood risk assessment. While remotely sensed observations have provided researchers with decades of continuous and reliable data for extracting flood information, it is important to note that relying solely on single-source remote sensing data may not provide a comprehensive solution for urgent flood monitoring. Using multi-source optical/SAR imagery can provide abundant spectral information for flood mapping.

## DATA

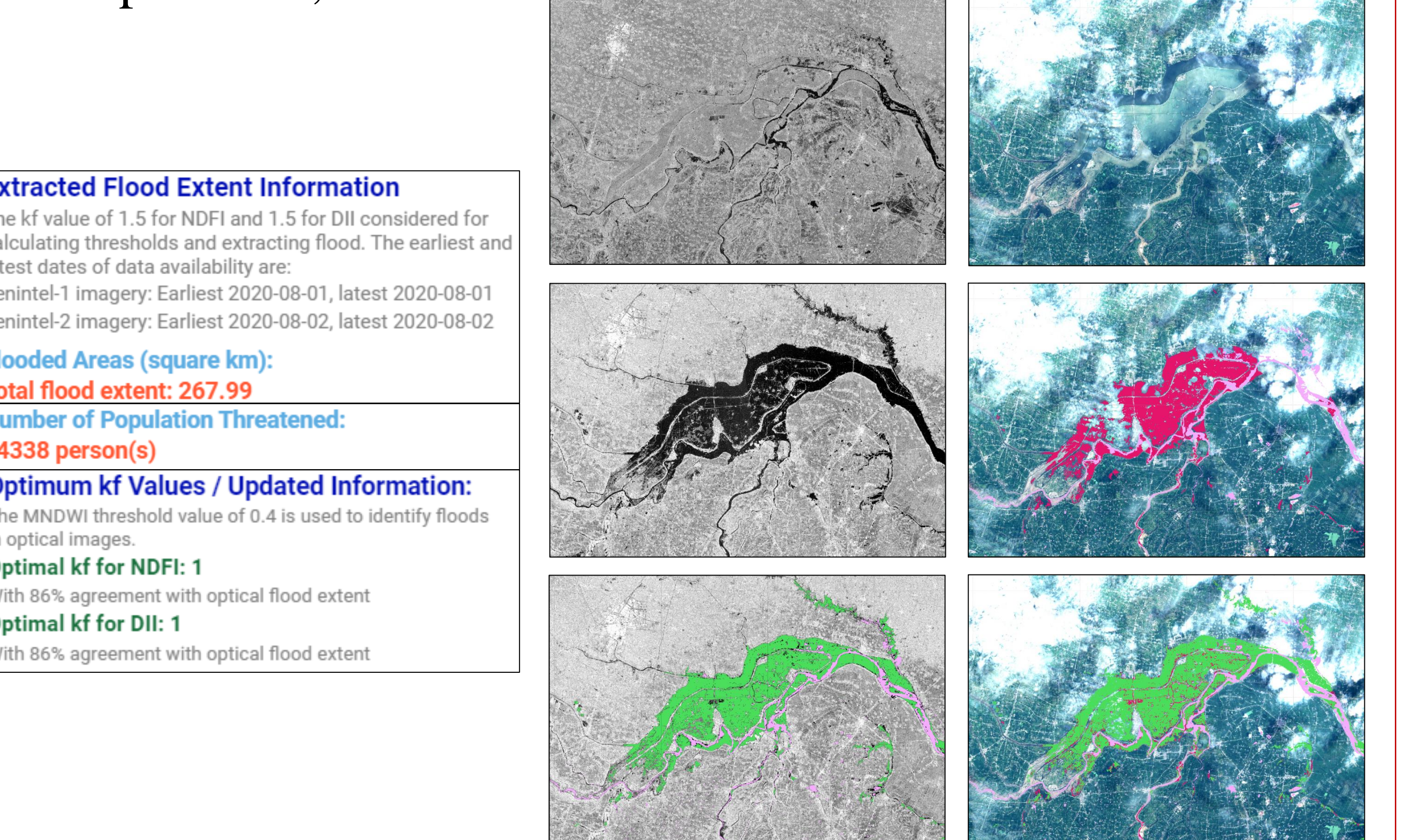
Data	Source	Resolution
Sentinel-1	"COPERNICUS/S1_GRD"	10 m
Sentinel-2	"COPERNICUS/S2"	20 m
LCLU	"USGS/NLCD_RELEASES/2019_REL/NLCD"	30 m
DEM	"NASA/NASADEM_HGT/001"	30 m
World Population	'WorldPop/GP/100m/pop'	100 m
Local Climate Zones	"RUB/RUBCLIM/LCZ/global_lc澤_map/latest"	100 m
Surface Water Mapping	"JRC/GSW1_0/GlobalSurfaceWater"	30 m

## METHODOLOGY

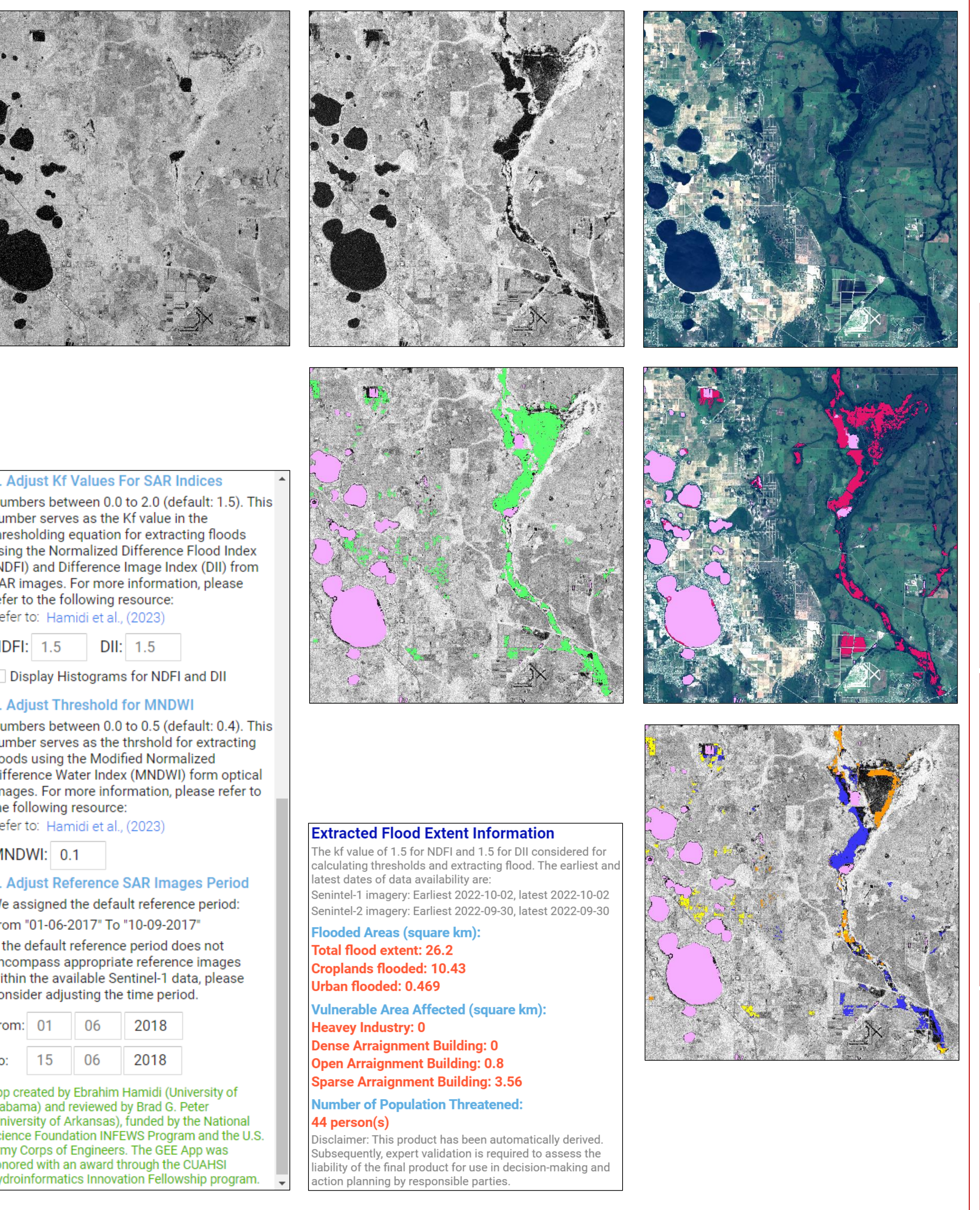


## RESULTS AND EXAMPLE

**Example 1:** Flood extent map after the July 20, 2020, event in Anhui province, China.

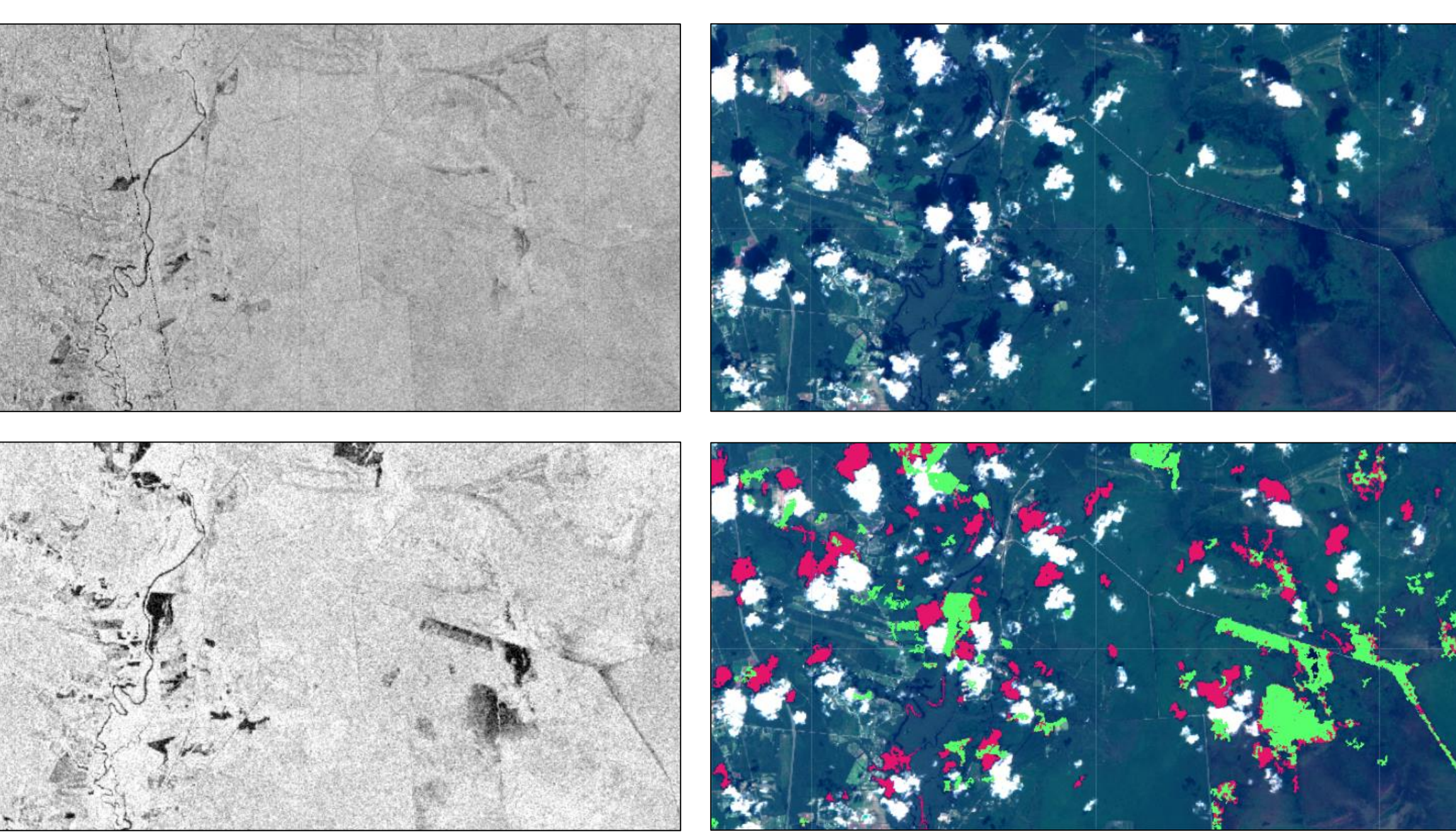


**Example 2:** The App is tested for the flood event following 2022 Hurricane Ian in Avon Park, Florida, U.S.



## RESULTS AND LIMITATION

**Example 3:** This case examines the flood event after 2018 Hurricane Florence around Northeast Cape Fear River, NC.



Cloud introducing errors into the calculation of optimum thresholds.

## CONCLUSION

This study leverages multi-source remote sensing resources and the capability of GEE to estimate flood extents rapidly. The App extracts diverse information from flood maps to assess critical supplementary details, expanding the agenda on flood-risk management to include economic, sociological, and geopolitical consequences.

## ACKNOWLEDGMENT

This study is funded by the National Science Foundation INFEWS Program (award #EAR-1856054), the U.S. Army Corps of Engineers (grant no. A20-0545-001). Also, partial support for development of this App is awarded through CUAHSI's 2023 Hydroinformatics Innovation Fellowship.

## REFERENCES

Hamidi, Ebrahim, Brad Peter, David F. Muñoz, Hamed Moftakhar, and Hamid Moradkhani, "Fast Flood Extent Monitoring With SAR Change Detection Using Google Earth Engine," in IEEE Transactions on Geoscience and Remote Sensing, vol. 61, pp. 1-19, 2023, Art no. 4201419, doi: 10.1109/TGRS.2023.3240097.

